NEW FUNCTIONAL FORMS AND PARAMETERIZATION METHODS FOR AB INITIO, INTERMOLECULAR FORCE FIELD DEVELOPMENT

by

Mary J. Van Vleet

A dissertation submitted in partial fulfillment of
the requirements for the degree of

Doctor of Philosophy

(Chemistry)

at the

UNIVERSITY OF WISCONSIN–MADISON

2017

Date of final oral examination: 08/15/17

The dissertation is approved by the following members of the Final Oral Committee:
J.R. Schmidt, Associate Professor, Chemistry
Clark R. Landis, Professor, Chemistry
Qiang Cui, Professor, Chemistry
Arun Yethiraj, Professor, Chemistry
Reid Van Lehn, Assistant Professor, Chemical and Biological Engineering

© Copyright by Mary J. Van Vleet 2017
All Rights Reserved

Soli Deo gloria.

ACKNOWLEDGMENTS

It is customary for authors of academic books to include in their prefaces statements such as this: "I am indebted to ... for their invaluable help; however, any errors which remain are my sole responsibility." Occasionally an author will go further. Rather than say that if there are any mistakes then he is responsible for them, he will say that there will inevitably be some mistakes and he is responsible for them....

Although the shouldering of all responsibility is usually a social ritual, the admission that errors exist is not — it is often a sincere avowal of belief. But this appears to present a living and everyday example of a situation which philosophers have commonly dismissed as absurd; that it is sometimes rational to hold logically incompatible beliefs.

— David C. Makinson (1965)

Above is the famous "preface paradox," which illustrates how to use the `wbepi` environment for epigraphs at the beginning of chapters. You probably also want to thank the Academy.

CONTENTS

LIST OF TABLES

LIST OF FIGURES

NEW FUNCTIONAL FORMS AND PARAMETERIZATION METHODS FOR AB INITIO, INTERMOLECULAR FORCE FIELD DEVELOPMENT

Mary J. Van Vleet

Under the supervision of Professor J.R. Schmidt
At the University of Wisconsin-Madison

FIXME: basically a placeholder; do not believe

I did some research, read a bunch of papers, published a couple myself, (pick one):

1. ran some experiments and made some graphs,
2. proved some theorems

and now I have a job. I've assembled this document in the last couple of months so you will let me leave. Thanks!

J.R. Schmidt

ABSTRACT

FIXME: basically a placeholder; do not believe

I did some research, read a bunch of papers, published a couple myself, (pick one):

1. ran some experiments and made some graphs,
2. proved some theorems

and now I have a job. I've assembled this document in the last couple of months so you will let me leave. Thanks!

PUBLISHED WORK AND WORK IN PREPARATION

---

[40] Van Vleet, M. J.; Misquitta, A. J.; Stone, A. J.; Schmidt, J. R. *J. Chem. Theory Comput.* **2016**, *12*, 3851–3870.

Part I

Introduction

1.1 The Importance of Molecular Simulation

This ref[2] is super cool!

What is molecular simulation? What types of problems can it solve? How does molecular simulation work? (Be sure to include solving Newton's EQs of motion and relevant details on the partition function and interaction energies!)

2.1 Molecular Mechanics and the Theory of Intermolecular Forces

What is a force field? What are the important components of a force field, and how do we model them?

2.1.1 The Many-Body Expansion

How do we break apart a force field into manageable pieces? Why does it make sense to break a force field into 2- and many-body components?

2.1.2 Energy Decomposition Schemes

Intramolecular Interactions

Brief commentary on the non-intermolecular portions of a force field

Electrostatics

Conceptual description of electrostatics: long-range multipoles and charge penetration

Exchange

Quantum-mechanically-based Pauli Exclusion. Theoretical grounds for exponential behavior

Induction

Charge transfer. Polarization. Polarization Damping.

Dispersion

Theoretical Formulation. Damping.

2.2 Ab-Initio Force Field Development

2.2.1 Electronic Structure Benchmarks

SAPT

General SAPT methodology. DFT-SAPT.

Coupled-Cluster Methods

CCSD(T). CCSD(T)-f12.

2.3 ISA-based methods for force field development

What is ISA? How can ISA be used to generate parameters for intermolecular force field development? What progress has been made from this approach?

Part II

Published Work

3 ISOTROPIC AB INITIO FORCE FIELDS

4 ANISOTROPIC AB INITIO FORCE FIELDS

Part III

Unpublished Work

5 AB INITIO FORCE FIELDS USING LMO-EDA

5.1 Preface

The preceding sections have been devoted to a development of various methodologies for ab initio intermolecular force field development, all generally assuming that Symmetry-Adapted Perturbation Theory (SAPT) can be used as a benchmark electronic structure theory. Critically, and especially given the developments discussed in Chapter 4, we can now usually expect our model force field energies to be within ~1 kJ/mol of the SAPT reference values! In spite of this success, this high precision between the model and SAPT energies can only lead to experimentally-accurate molecular simulation provided that the SAPT energies themselves are accurate, either with respect to the exact underlying potential energy surface (PES) or (in practice) with respect to gold-standard CCSD(T) calculations. Indeed, for systems where SAPT and CCSD(T) disagree by several kJ/mol, there is little point in developing SAPT-based force fields with sub- kJ/mol accuracy! This limitation raises to two fundamentally important questions. First, for what types of systems might we expect SAPT to be inaccurate? Second, for the systems where SAPT and the exact PES are in disagreement, how must we modify our typical methodology for ab-initio force field development?

The purpose of this chapter is to partially address these questions, all within the specific context of force field development for Metal-Organic Frameworks (MOFs). Note that the results presented here were gathered from 2012–2014, so some important advances (namely those presented in Chapters 3 and 4) haven't been incorporated into the force fields presented here. This is probably to the determinent of the accuracy and transferability that might be possible with the LMO-EDA-based methodology, and (should this project be picked up in the future) it may be necessary to refit these force fields to the functional forms and monomer-based parameters discussed in Chapter 4.

5.2 Introduction

Metal-Organic Frameworks (MOFs) are an increasingly important class of compounds that are defined as porous materials which contain inorganic nodes connected by organic linkers. Within this general motif, more than 20,000 compounds have been reported and studied,[3] and this vast diversity of MOF materials shows great promise for chemical customization and optimization. Within the past two decades, a huge body of research has been devoted to the design and study of MOFs, and current applications range from gas separation and storage to catalysis and biomedical imaging.[3]

Somewhat recently, it has been discovered that so-called Coordinatively-Unsaturated (CUS) MOFs can be created by activation of solvent-coordinated inorganic nodes to yield exposed (or 'open') metal sites.[4–6] These CUS-MOFs have been shown to exhibit exhibit excellent uptakes and selectivities in a number of gas separation and storage problems,[4,5,7] making this family of compounds an excellent target for future investigation and materials design. Owing to the vast scope of hypothetical CUS-MOF materials, however, and the number of chemically-distinct targets for gas separation/storage, it is unlikely that experiment alone can be used to screen for new and promising CUS-MOF materials.[8] Rather, a combination of experiment and computational modeling will be required to find (or possibly even rationally design) optimal CUS-MOFs.[7–9]

Despite the utility of computational studies, it remains challenging to develop molecular models for CUS-MOFs.[6] Because the strong binding between metal and adsorbate leads to chemical environments substantially different from typical coordinatively-saturated MOFs, many standard force fields (such as UFF and DREIDING) which yield good predictions for these MOFs frequently (and substantially!) underpredict adsorption in CUS-MOFs, especially at low pressures.[8–10] While CUS-MOFs can sometimes be studied using quantum mechanical means,[9,11] clearly new and improved force fields will be required to perform in-depth simulations and large-scale screenings of these materials.

The goal of the present chapter is to present a general methodology for devel-

oping accurate and transferable force fields for CUS-MOFs. The current study is limited to a discussion of the MOF-74 series (a prototypical and well-studied CUS-MOF), however it is expected that the methods presented herein might also be applicable to other systems. After outlining this methodology (Sections 5.3 and 5.4), we next show how our force fields can be applied to accurately predict CO_2 adsorption isotherms in Mg-MOF-74. At the present time, we do not have results for other compounds in the M-MOF-74 series (M = Co, Cr, Cu, Fe, Mn, Ni, Ti, V, and Zn), largely as a result of techical challenges in the force field parameterization itself. We discuss these technical challenges in some detail, and conclude with our perspective on the challenges and opportunities associated with developing transferable force fields for these and other CUS-MOF systems.

5.3 Background and Motivation

Prior work in our group has shown how, at least for coordinatively-saturated MOFs, accurate and transferable force fields can be generated for a wide variety of systems by fitting force field parameters on a component-by-component basis to reproduce an ab initio SAPT energy decomposition.[12,13] While full details for this force field development methodology can be found in Refs. 13, 14, a short workflow is as follows:

1. Generate a representative cluster model from which interaction parameters can be determined for each pairwise interaction. An example cluster, used to parameterize Mg–CO_2 interactions in Mg-MOF-74, is shown in Fig. 5.1.

2. Using DFT-SAPT (a variant of SAPT with monomer densities given by Density Functional Theory (DFT)), compute a series of representative dimer interaction energies for the model cluster. For the cluster model in Fig. 5.1, representative dimers were generated by varying the position of CO_2 with respect to the MOF cluster, and the corresponding DFT-SAPT total interaction energies are shown for a subset of representative points.

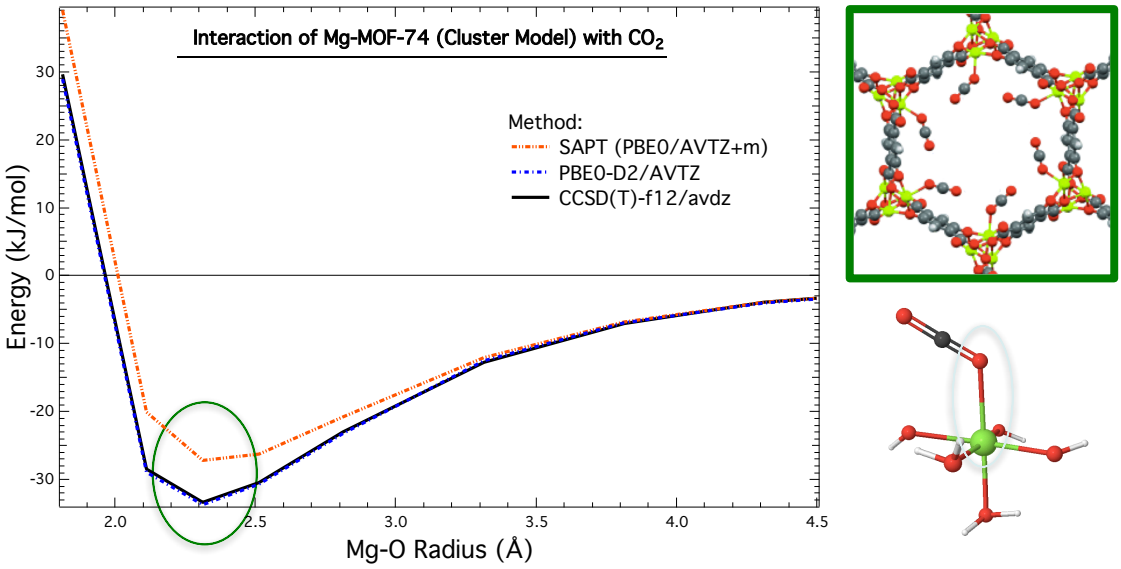

Figure 5.1: Model PES for interactions between CO_2 and Mg-MOF-74. (Left) Interaction energies between CO_2 and a cluster model of Mg-MOF-74 (shown bottom right), computed at a CCSD(T)-f12 (black), SAPT (orange), and/or PBE0-D2 (blue) level of theory. Discrepancies between SAPT and CCSD(T)-f12 in the minimum-energy region of the potential have been highlighted. (Top right) The structure of CO_2-bound Mg-MOF-74. (Bottom right) The structure of the cluster model used for Mg-MOF-74, where the circled atom pair indicates the relevant Mg-O radius from the x-axis in the leftmost figure.

3. To determine partial charges for the system, generate representative clusters (as described in Section 5.5) for each the organic ligand and the inorganic node, and perform a Distributed Multipole Analysis (DMA) analysis on each cluster to determine partial charges for the overall system.

4. For each component of the DFT-SAPT interaction energy, parameterize the relevant functional forms (as detailed in Ref. 13 and Section 5.4) to reproduce the DFT-SAPT component energy.

Once parameterized, these SAPT-based MOF force fields can be used for calculating individual adsorption isotherms or even for high-throughput screening.[14]

In the generation of force fields for CUS-MOFs, we expect that many of the advantages of the above workflow for coordinatively-saturated MOFs (such as the component-by-component based parameterization and method for partial charge determination) will also translate well to CUS-MOF materials. Nevertheless, there are two reasons why a SAPT-based methodology cannot be used to generate such force fields. First, and as shown in Fig. 5.1 for a representative Mg-MOF-74 cluster model, we have empirically found SAPT to be in error for CUS-MOF-like systems compared to benchmark CCSD(T)-f12 calculations. DFT-SAPT has been known to struggle with highly ionic systems (relative to CCSD(T) or DFT methods),[15,16] and so this error is perhaps not surprising. (Possible sources of the discrepancy between SAPT and CCSD(T)-f12 will be discussed in Section 5.8.) Nevertheless, and in the absence of fortuitous error cancellation, predictions from an ab initio force field can only be as good as the level of theory that they are parameterized against. Consequently, because SAPT underbinds CO_2 by a full 6 kJ/mol compared to CCSD(T)-f12, we would not expect to see good predictions for the CO_2 adsorption isotherm with a SAPT-based methodology, and a new strategy will be required.

As a second barrier to using a SAPT-based methodology, many of the compounds in the M-MOF-74 series are open-shell. Though this poses no fundamental issue, in practice most implementations of SAPT (aside from the seldom-used SAPT 2012 package developed in Krzysztof Szalewicz's group at Delaware) do not allow for computations of open-shell systems, and indeed SAPT-based studies of open-shell compounds are very rare.[17] For these reasons, a new, open-shell-compatible electronic structure benchmark is highly preferable.

5.4 New Methods for CUS-MOF force fields

Based on the results for Mg-MOF-74, it is clear that, at least for CUS-MOFs, a new methodology is required which simultaneously keeps the important advantages of the old workflow (especially the component-by-component based parameterization, which is essential for generating transferable force fields) while overcoming the limitations of SAPT itself. Put differently, for CUS-MOFs we should seek a

new electronic structure theory benchmark and associated Energy Decomposition Analysis (EDA) with the following qualities:

1. High accuracy with respect to to CCSD(T)-f12 benchmark energies
2. Physically-meaningful energy decomposition into (at least) electrostatics, exchange, induction, and dispersion
3. For systems where SAPT and CCSD(T)-f12 agree, a quantitative correspondence between the energy decompositions of SAPT and the new method

Assuming these three qualites are met, we expect to be able to generate force fields for CUS-MOFs that are both highly accurate and maximally-compatible with previous force fields developed for coordinatively-saturated MOF systems.

A substantial number of EDAs exist in the literature, and the interested reader is referred to Ref. 16 for a review and comparison of various popular methods. Aside from SAPT, which is a perturbative method, most EDAs are 'variational', meaning that the various energy components are calculated in stages from a series of constrained relaxations of the monomer wavefunctions into the optimized dimer wavefunction. For this reason, all variational EDAs are guaranteed to have total energies that match the result from a supermolecular interaction energy calculation. Furthermore, these EDAs are often implemented for wavefunction and DFT methods, thus allowing for significant flexibility (compared to the SAPT EDA) in terms of finding an EDA whose total energy closely matches CCSD(T)-f12. Indeed, and as shown in Fig. 5.1, PBE0-D2 shows excellent agreement with CCSD(T)-f12 for a Mg-MOF-74 cluster model, and so any DFT-compatible EDA should meet our first criteria from above.

Although all variational EDAs yield the same total interaction energy for a given level of theory, many EDAs can differ substantially in terms of how this total energy is decomposed into chemically-meaningful components. At the time this research was completed, only a handful of variational EDAs distinguished each electrostatics, exchange, induction, and dispersion. (Notably, the recent second-generation ALMO-EDA[18] now separates their 'frozen' energy term into electrostatic, exchange, and

dispersion components, and might thus might be worth re-investigation.) Of the popular EDA methods available as of 2014, we found that LMO-EDA,[19,20] GKS-EDA,[21] and PIEDA[22] decompose the total interaction in a manner philosophically similar to SAPT, and include each electrostatic, exchange, induction, and dispersion terms. These three methods thus meet our second criteria for an optimal energy decomposition scheme for CUS-MOFs, and complete formalisms and details for the methods can be found in Refs. 19–22.

As for the last criterion, that of maximum correspondence between SAPT and a variational EDA, we have performed component-by-component analyses to compare SAPT to both LMO-EDA and GKS-EDA. PIEDA is known to overestimate the relative magnitude of the polarization energy, compared to SAPT, and thus was not considered in detail.[16] As for LMO-EDA and GKS-EDA (both of which are based on very similar theories, and tend to yield similar energy decompositions), we have in general found semi-quantitative to quantitative agreement with the SAPT energy decomposition, particularly for the electrostatic and exchange energies. Comparisons between LMO-EDA and SAPT are shown for the CO_2 dimer (Fig. 5.2) and for CO_2 interacting with a model Mg-MOF-74 compound (Fig. 5.3). GKS-EDA results are not shown, as the LMO-EDA and GKS-EDA results tend to be very similar, with the GKS-EDA results in slightly worse agreement with SAPT. For this reason, and because LMO-EDA does the best job of meeting our three criteria above, we choose in this work to use LMO-EDA as our new benchmark EDA for fitting CUS-MOF force fields.

In addition to describing the advantages of the LMO-EDA method, it is worthwhile to overview some of its relevant shortcomings, and limitations. As with most variational EDA methods,[16] and especially for DFT-based methods, it becomes difficult to precisely assign and separate out the true 'dispersion' energy for a system. This limitation is also true of LMO-EDA, where the dispersion energy is defined as the difference in correlation energy between the monomer and dimer wavefunctions. For density functionals employing Grimme's –D dispersion correction, this correction is also added to the LMO-EDA dispersion energy. For functionals that have a well-defined and theoretically-grounded distinction between the

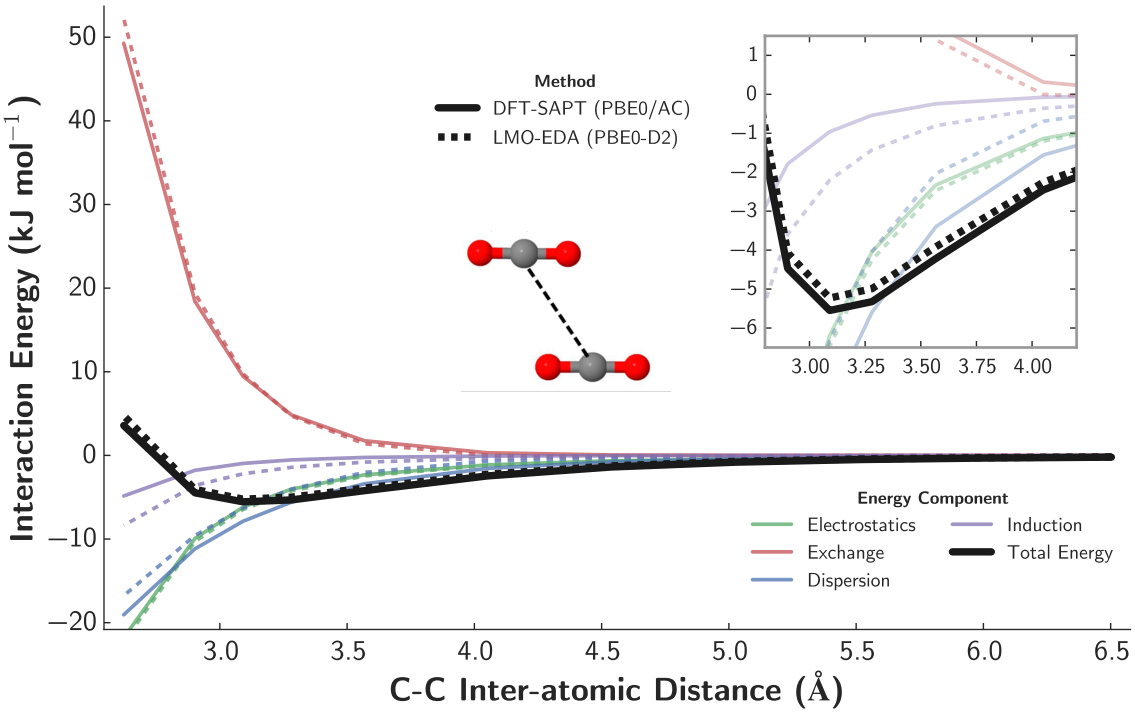

Figure 5.2: PES and associated energy decomposition for the slipped parallel geometry of the CO_2 dimer as a function of the C–C interatomic distance. The PES has been computed by both DFT-SAPT (PBE0) (solid lines) and LMO-EDA-PBE0-D2 (dashed lines), and each electrostatics (green), exchange (red), dispersion (blue), induction (purple), and total energy (black) components are displayed. Note that, for the DFT-SAPT energies, the δHF contribution has been incorporated into the induction energy.

exchange and correlation functionals, the LMO-EDA energies tend to agree well with SAPT, and we have found good agreement (for instance) between SAPT and LMO-EDA-PBE0-D2. With other functionals, such as with our tests using the M06 functional, there is no separation between the exchange and correlation functionals, and LMO-EDA gives unphysical values for both the exchange and dispersion energies in this case. (GKS-EDA attempts to rectify this issue by changing the LMO-EDA formalism for dispersion. While this leads to qualitative agreement between SAPT and GKS-EDA for a wider variety of functionals, the quantitative agreement for

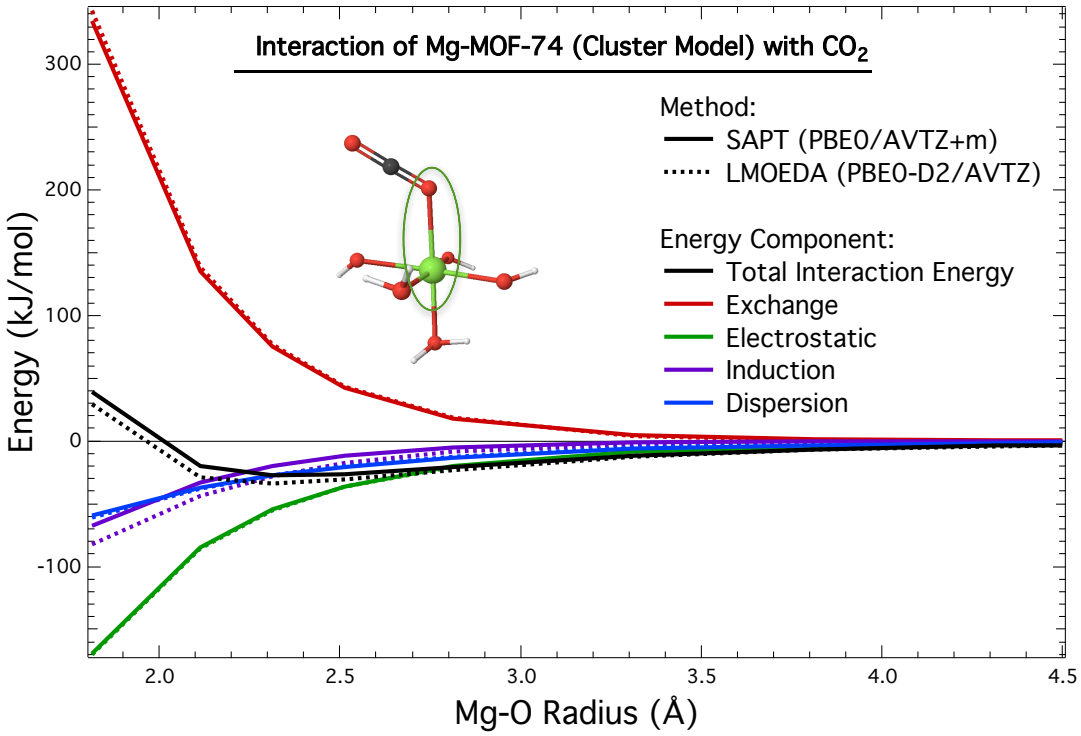

Figure 5.3: PES and associated energy decomposition for a CO_2 + MgO_5 cluster, as a function of the highlighted Mg–O interatomic distance. The PES has been computed by both DFT-SAPT (PBE0) (solid lines) and LMO-EDA-PBE0-D2 (dashed lines), and colors and labels for the energy decomposition are as in Fig. 5.2.

the PBE0-D2 functional is somewhat worsened for the systems studied herein, and we instead use LMO-EDA-PBE0-D2 for all results in this work.)

A second, and purely practical, limitation of LMO-EDA is its memory-intensive implementation in GAMESS. As will be discussed in detail later, calculations on a large (43 heavy atom) cluster model of Mg-MOF-74 were infeasible for us (using the Phoenix cluster in 2014) in all but the smallest VDZ basis set, and calculations on an identical cluster model of Co-MOF-74 could not be completed at all. For this reason, the LMO-EDA method is practically restricted to studies of smaller systems and/or basis sets.

5.5 Computational Methods

5.5.1 Partial Charge Determination

Partial charges for Mg-MOF-74 were determined in a manner analagous to Ref. 14 using the Q_{SBU} method. Two cluster models, one a hydrogen-capped DOBDC ligand environment, and one a capped MgO_5 inorganic chain, were constructed and analysed using a Distributed Multipole Analysis (DMA). The resulting DMA charges were then used to obtain charge paramters for the ligand and inorganic SBU, respectively. See Section 5.A for final charge parameters.

5.5.2 Force Field Fitting

Two types of force field functional forms were considered in this work. The first, a 'single-exponential' functional form, exactly matches that used in Ref. 23, with the exception that δHF parameters were not fit to the Mg atomtype. This fitting choice was due to the fact that LMO-EDA only provides a total induction term (rather than splitting into 2^{nd}- and higher-order induction energies, as with SAPT).

For the 'double-exponential' functional form used to fit the Mg-MOF-74-Yu cluster model, the same functional form was used as in the single-exponential case, with the exception that two sets of short-range interaction parameters (labeled Mg and Du in Section 5.A) were assigned to the Mg atomic center. This effectively meant that Mg was described by two separate exponential decays, which enabled the much more accurate force field fits discussed in Section 5.6.

In all cases, force fields were fit using the Fortran code described in the Appendix of Ref. 24.

5.6 Results

5.6.1 Initial Force Field and Cluster Model Analysis

Originally, we attempted to fit Mg parameters on the basis of a small, 6 heavy atom cluster ('Mg-MOF-74-small', see Fig. 5.4 for chemical structure), which we felt would be representative of the Mg environment in Mg-MOF-74. Using the functional forms discussed in Section 5.5, force field parameters were fit to reproduce LMO-EDA-PBE0-D2 energies for a variety of CO_2/Mg-MOF-74-small interactions, with results shown in Fig. 5.4. Though some interaction energies disagree by several kJ/mol between LMO-EDA-PBE0-D2 and the force field energies, overall the agreement is reasonable, and the force field correctly reproduces trends in the interaction energies without significant systematic error.

Based on the agreement between PBE0-D2 and the force field, as well as between PBE0-D2 and CCSD(T)-f12, we expected to obtain good CO_2 adsorption isotherm predictions for the Mg-MOF-74 system itself. By contrast, our computed isotherm substantially underpredicts the experimental adsorption at low pressures, where Mg–CO_2 interactions are known to dominate. This underprediction strongly suggests that we had originally underestimated the magnitude of the Mg–CO_2 binding, a result which we were then able to attribute to our choice of cluster model (vida infra).

Cluster models for the M-MOF-74 series have been investigated by several groups, and it has been found in general that computed binding energies are sensitive both to the size of the cluster model as well as the treatment of geometry relaxation effects.[26,27] Consequently, we calculated the CO_2 binding energies and geometries of both our original Mg-MOF-74-small cluster as well as for two larger clusters developed in Refs. 6, 25. These latter two clusters, respectively denoted Mg-MOF-74-Yu and Mg-MOF-74-Dzubak, are the same size (each with 60 atoms), but have made different choices as to the number of included magnesium atoms (three vs. four) and number/location of capping atoms. To test the influence of model cluster on the CO_2 binding energy/geometry, we performed two sets of

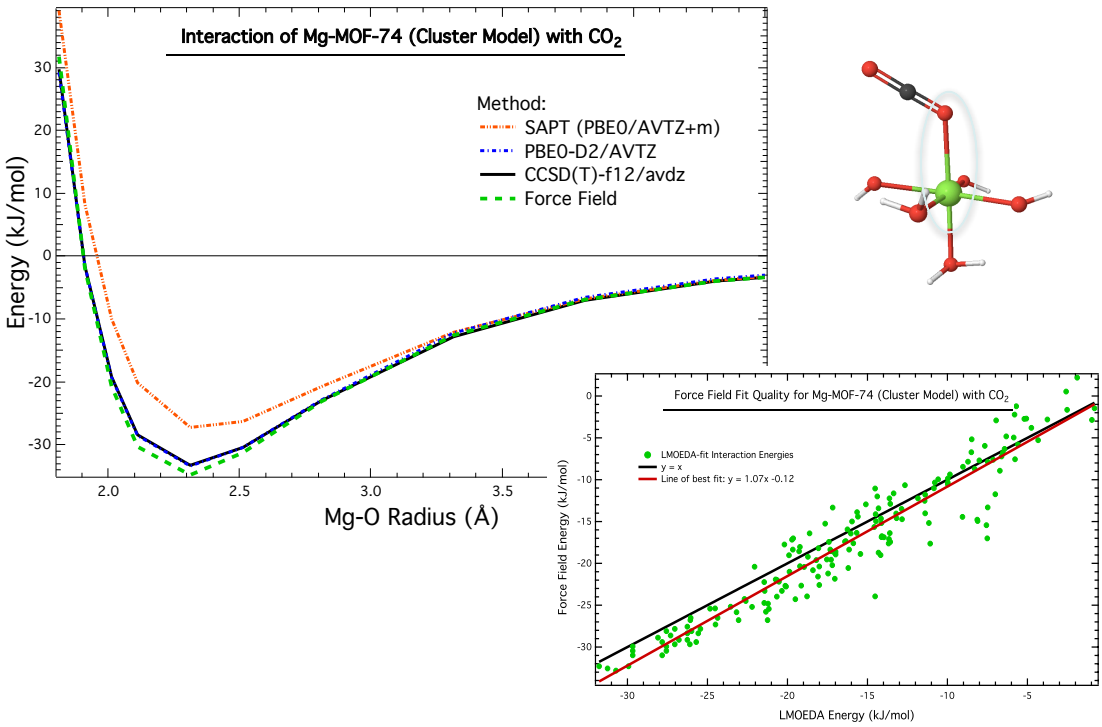

Figure 5.4: Force field fitting quality for the Mg-MOF-74-small cluster. (Top left) Various electronic structure benchmarks for Mg-MOF-74-small along with the classical potential. Each DFT-SAPT (orange dot-dashed), PBE0-D2 (blue dot-dashed), CCSD(T)-f12 (black solid), and the LMO-EDA-based force field (green dashed) are shown as a function of the Mg–O interatomic distance (non-bonding pair highlighted at top right). (Bottom right) Force field fit quality, as benchmarked against LMO-EDA-PBE0-D2, for a semi-random set of dimer configurations of the Mg-MOF-74-small cluster model interacting with CO_2. The black line establishes the $y = x$ benchmark, and the red line represents the line of best fit.

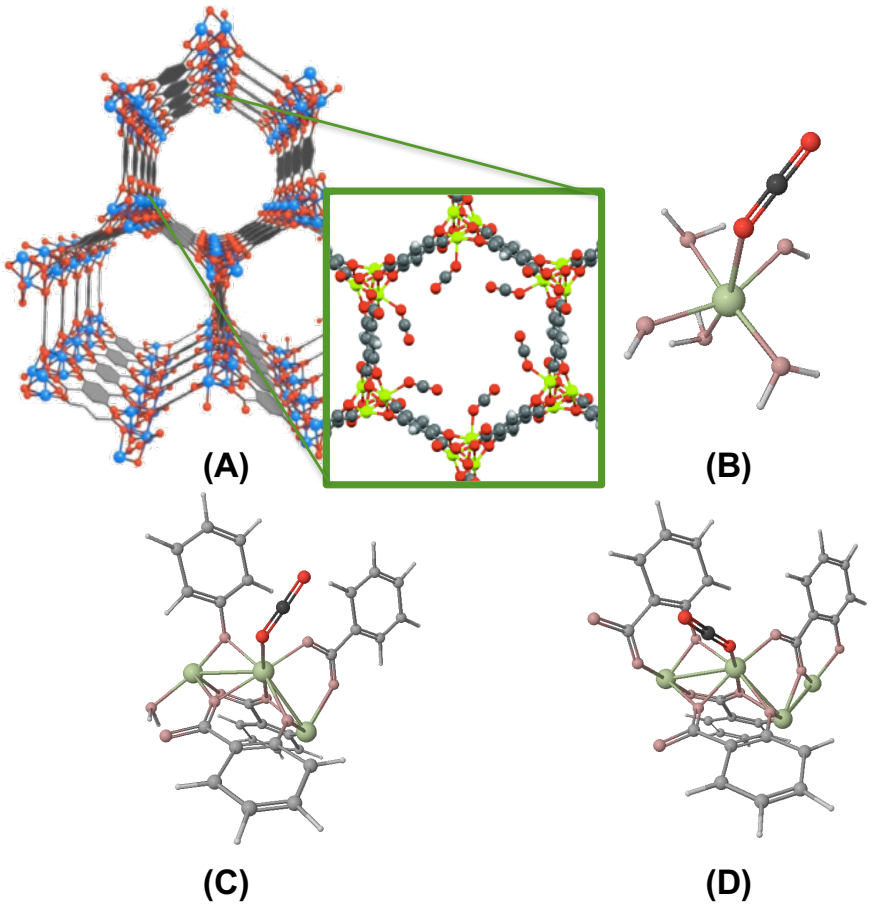

Model	CO_2 Binding Energy (kJ/mol)	Mg–O Interatomic Distance (Å)	Mg–O–C Tilt Angle (°)
A[11]	**-41.5**	**2.31**	**129**
B	-23.3	2.31	122
C	-31.4	2.28	123
D	-41.7	2.20	149

Figure 5.5: Various structures and cluster models for Mg-MOF-74 interacting with CO_2. (A) Full periodic Mg-MOF-74 structure with inset showing adsorbed CO_2 positions. (B) Mg-MOF-74-small cluster, containing 6 heavy atoms (not including CO_2). (C) Yu et al. cluster model for Mg-MOF-74, denoted in text as Mg-MOF-74-Yu. (D) Dzubak et al. cluster model for Mg-MOF-74, denoted in text as Mg-MOF-74-Dzubak. All cluster models as shown with optimized CO_2 positions, and bond lengths and angles for adsorbed CO_2 are given in the bottom table. Data for (A) was taken from Valenzano et al. using a B3LYP-D level of theory,[11] whereas data for (B-D) was computed in this work using PBE0-D2. Finally, note that the binding energy for (A) includes framework geometry relaxation effects, whereas (B-D) were computed using semi-rigid cluster geometries and only optimizing the CO_2 position and exposed MgO_5 pocket.

optimizations of the Mg-MOF-74-Yu and Mg-MOF-74-Dzubak clusters: one in which only the CO_2 position was optimized, and one in which the exposed MgO_5 pocket was additionally relaxed. Binding geometries were relatively insensitive to the geometry relaxation, though binding energies varied by 2-5 kJ/mol, in agreement with other studies that have tested geometry relaxation effects.[26] Results for the $CO_2 + MgO_5$ relaxation are shown in Fig. 5.5.

Of the three studied cluster models, both Mg-MOF-74-small and Mg-MOF-74-Yu correctly reproduce the Mg–O interatomic distance and Mg–O–C tilt angle. These geometrical parameters arise primarily from electrostatic interactions between CO_2 and the MgO_5 pocket,[11] suggesting that both of these models capture such important interaction features. By contrast, the Mg-MOF-74-Dzubak model predicts a substantially shorter binding distance and increased tilt angle, both in contrast to results from the periodic system. In part, these deficiencies can be attributed to spurious CO_2 interactions with the exposed carbonyl capping groups in the Mg-MOF-74-Dzubak model which are not present in the periodic system or the other two cluster models. Additionally, a Mulliken charge analysis of the Mg-MOF-74-Dzubak cluster yields larger partial charges for the surrounding Mg atoms as compared to the Mg-MOF-74-Yu model, which may help explain the increased binding and shortened Mg–O contact in the Mg-MOF-74-Dzubak model. As for binding energies, there are substantial differences in binding energies between the various cluster models, with Mg-MOF-74-small severely underbinding These results for the Mg-MOF-74-small cluster indicate the inadequacy of such a small model, and likely explain the underprediction of the CO_2 adsorption isotherm from above. The Mg-MOF-74-Dzubak model shows best energetic agreement with the periodic system. Nevertheless, some of the Mg-MOF-74-Dzubak binding energy arises from truncation effects (as described above), and the energetic agreement is thus due (at least in part) to error cancellation. Indeed, some of the binding energy in the periodic system arises from (attractive) long-range interactions, and thus we should expect to see a cluster model somewhat underpredict the binding energy. Primarily for its good agreement in binding geometries, and reasonable agreement in binding energy, we opt to use the Mg-MOF-74-Yu cluster model for

the remainder of this work.

5.6.2 Final Mg-MOF-74 CO_2 Adsorption Isotherm

Using our new Mg-MOF-74-Yu cluster model, we next attempted to fit new force field paramters for Mg. As discussed earlier, and because of the size of this new cluster (60 atoms), LMO-EDA-PBE0-D2 calculations became cost prohibitive in all but the smallest VDZ basis set and for a limited set of points. Starting from the minimum energy configuration shown in Fig. 5.5, we fit Mg parameters to a 12-point scan along the Mg-O bond vector, with fit results shown in Fig. 5.6. Interestingly, though the functional form used in this fit was sufficient to accurately paramterize the interaction energies in the Mg-MOF-74-small cluster, the same force field methodology proved unsuccessful in paramterizing Mg-MOF-74-Yu interactions. We knew at the time that this inaccuracy was probably a consequence of uncertainties in correctly parameterizing the Mg short-range exponent. (See Chapter 3 for a full discussion of new methods for parameterizing the short-range potential.) Nevertheless, because the Slater-ISA methodology for short-range interactions had not yet been developed, we opted instead to fit the Mg interactions to a double exponential functional form, with each exponent corresponding to the ionization potential for either Mg^+ or Mg^{2+}, the two chemical environments that we thought might correctly represent the Mg cation. As shown in Fig. 5.6, this form could excellently reproduce the Mg-MOF-74-Yu model PES.

Using the double exponential functional form from above, we recomputed the Mg-MOF-74 CO_2 adsorption isotherm. Before comparing to experiment, and as recommended by others,[28] we scaled the experimental isotherm in order to account for the pore blocking effects that are common in the M-MOF-74 series. Using this scaled isotherm, we then obtain excellent agreement between our model potential and experiment (Fig. 5.7). Crucially, this accuracy is seen both at low- and high-pressure ranges, indicating the accuracy of the force field in modeling both the strong Mg–CO_2 binding as well as the weaker physisorption regime.

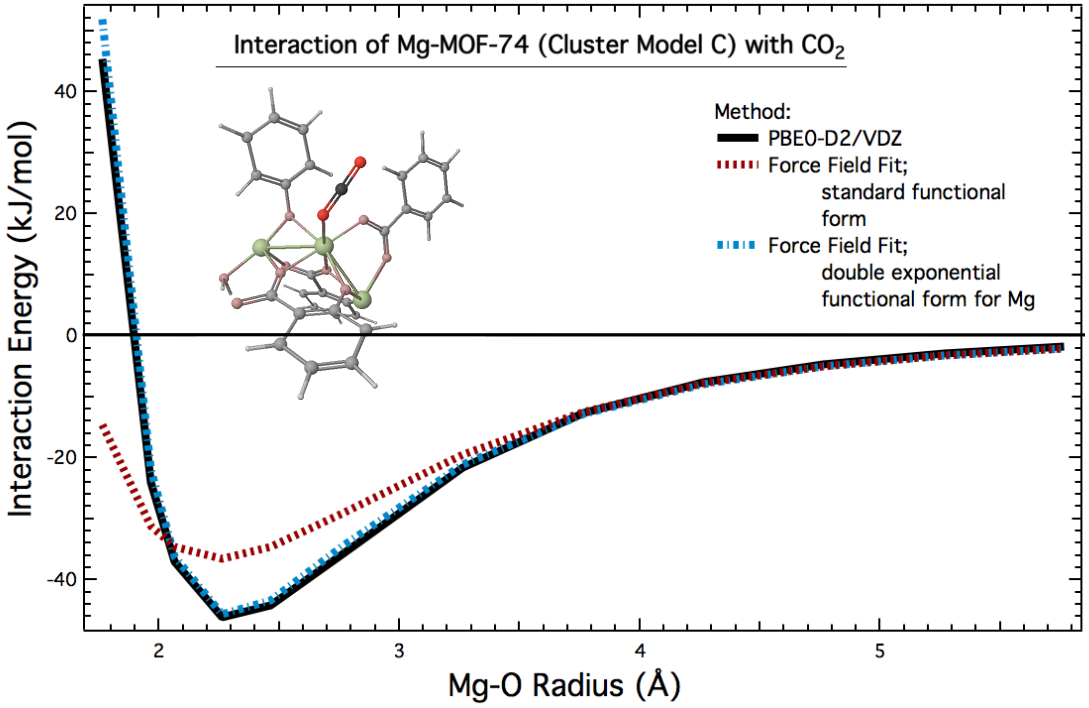

Figure 5.6: Force field fitting quality for the Mg-MOF-74-Yu cluster. A PBE0-D2 benchmark (black solid) is displayed along with two force field fits: single-exponential (red dashed) and double-exponential for Mg (blue dash-dotted). In either case, a cut of the PES is shown along the interatomic distance between the central Mg atom and the closest-contact oxygen atom in CO_2.

5.6.3 Transferability to Other Adsorption Isotherms

In addition to using our Mg paramters to compute the CO_2 adsorption isotherm, we also used our Mg force field in conjunction with the N_2 parameters developed by Yu et al.[29] to predict the N_2 adsorption isotherm. These predictions were generally poor, and results are not shown. Nevertheless, the poor N_2 results suggest a lack of transferability of our Mg parameters, possibly (and as discussed in the section on Future Work) due to unphysical double-exponential functional form used to parameterize Mg.

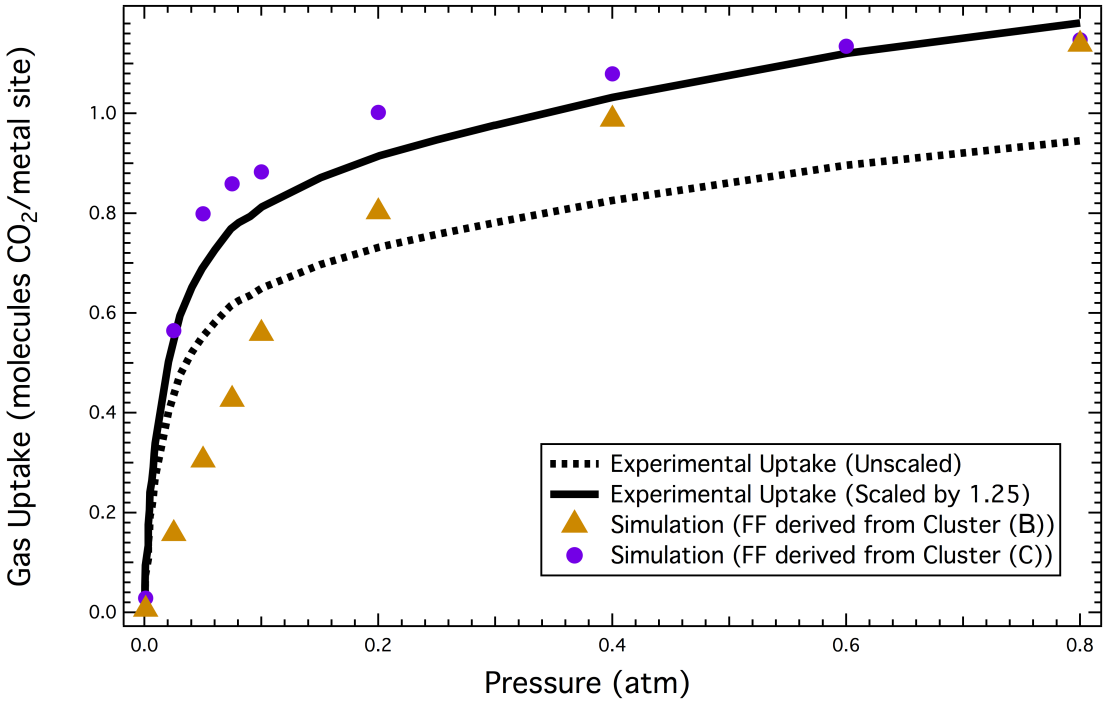

Figure 5.7: Predicted CO_2 adsorption isotherm for Mg-MOF-74. Two experimental isotherms are shown, one as directly measured by experiment (dashed line) and one scaled to account for pore block effects (solid line). Predictions from two force fields are also shown, where Mg parameters for each force field were fit either to the Mg-MOF-74-small cluster (gold triangles) or to the Mg-MOF-74-Yu cluster (purple circles). Cluster geometries are given in **??**.

5.6.4 Transferability to Other M-MOF-74 systems

As a second test of transferability, we also attempted to develop force fields for other compounds in the M-MOF-74 series, starting with Co-MOF-74. Unfortunately, the open-shell nature and increased electron count of Co-MOF-74 made LMO-EDA calculations computationally prohibitive for any reasonable basis set, and these systems were not investigated further.

5.7 Conclusions

In this unpublished work, we have determined a new methodology for fitting force fields to CUS-MOFs. While largely following our previous methodology for MOF force field development, we have shown how an LMO-EDA Energy Decomposition Analysis can be used in leiu of SAPT to generate accurate ab initio benchmark energies in cases where SAPT itself is inaccurate. Using this new methodology, we have successfully modeled CO_2 interactions in Mg-MOF-74, and have simulated the adsorption isotherm for CO_2 in Mg-MOF-74 with good accuracy compared to experiment.

Ultimately, the methods presented herein suffered from a number of practical and fundamental issues (see Section 5.8. Unless these limitations can be fully addressed, we do not anticipate that the LMO-EDA method can be broadly used to develop force fields for CUS-MOFs or other large systems where SAPT is in error.

5.8 Future Work

Throughout this manuscript, we have attempted to highlight some of the key limitations of our force field development methodology for CUS-MOFs. In summary, the following issues would need to be resolved in order to expand the scope of the present research:

1. **Memory Limitations in GAMESS**: As evidenced in this work, relatively large (60+ atom) cluster models are required to correctly parameterize force fields for the M-MOF-74 system. While these cluster sizes do not present difficulties for standard DFT calculations with reasonable basis sets, the corresponding LMO-EDA calculations were, as implemented in the GAMESS software package, infeasible due to memory requirements. Some time was spent attempting to address these memory issues, particularly for the memory-intensive Edmiston-Ruedenberg localization subroutine that is the source of the problem. However, due to our lack of familiarity with the GAMESS software and the LMO-EDA source code, this pursuit was eventually dropped.

2. **Fundamental Issues with LMO-EDA**: As discussed in Section 5.4, the LMO-EDA method has several theoretical limitations. In particular, and especially for functionals with no defined separation between exchange and correlation functionals, LMO-EDA does not offer a clean separation between the exchange and dispersion energies. Furthermore, and unlike some recent EDA methods, LMO-EDA cannot separate induction into charge transfer and polarization components.

3. **Transferability of the Force Field Functional Form**: While our final force field for studying CO_2 interactions in Mg-MOF-74 was highly accurate (both with respect to ab initio theory and with respect to experiment), it does not appear that this accuracy extends to models for the adsorption of other small molecules, such as N_2. This transferability limitation is almost certainly due to the chosen double-exponential functional form and/or the parameterization process used to obtain Mg parameters, and improvements to this methodology will be essential to make our work on the CO_2-Mg-MOF-74 system applicable to general force field development for CUS-MOFs. In particular, we will require a better force field for describing short-range interactions, as the functional forms and paramters used in this work struggled to model the Mg-MOF-74 exchange energies.

While several of these issues (particularly practical limitations with the LMO-EDA implementation) have yet to be addressed in a meaningful fashion, several recent theoretical advances may pave the way for continued work on this project. Thus for CUS-MOFs and other systems where DFT-SAPT might be in error, we offer the following recommendations:

1. **Improved SAPT energies**: Recently, it has been proposed that the commonly used single-exchange (" S^2") approximation can lead to errors in the description of the induction energy,[30] particularly for ionic systems.[15] While it is difficult to attribute errors in SAPT to a particular energy component, it may well be that SAPT poorly describes Mg-MOF-74 due to the S^2 treatment of

the induction energy. In this case, eliminating the S^2 approximation might improve the DFT-SAPT total interaction energies, thus enabling SAPT to be used for (at least) closed-shell CUS-MOFs.

2. **New SAPT Correction Schemes**: As discussed in Chapter 4, deviations between SAPT and CCSD(T) can be rectified by adding a δCCSD(T) correction to the total SAPT energy. Thus far, we have had good success modeling this δCCSD(T) correction as part of the dispersion energy, though this is an empirically-justified choice, and may need modification for treating Mg-MOF-74. Regardless, the results in Chapter 4 indicate that correcting (rather than entirely ignoring) the DFT-SAPT energies is a promising strategy for transferable force field development.

3. **New EDA schemes**: Since this work was completed, a second-generation ALMO-EDA scheme has been implemented in the Q-Chem software package.[18] Crucially, and unlike its predecessor, this ALMO-EDA scheme now breaks up the interaction energy into electrostatic, exchange, polarization, charge-transfer, and dispersion components. While there is no guarantee that such an EDA could serve as the basis for CUS-MOF force field development (see Section 5.4), these and other recently developed EDAs may be worth investigation, and could eventually replace the (practically problematic) LMO-EDA method.

4. **Improved Force Field Functional Forms**: Since 2014, we have made significant progress in developing more accurate and transferable intermolecular force fields (see Chapters 3 and 4), and many of these advances particularly improve the description of the short-range potential itself. There is a good chance that either the Slater-ISA FF or MASTIFF methodologies would yield high-quality force fields for Mg-MOF-74 and other systems. In this case, continued work on this project might be an exciting avenue for showcasing the MASTIFF methodology in the context of accurate inorganic/organometallic force field development.

5.A Force Field Parameters for CO_2 and Mg-MOF-74

Final force field parameters, fit using the double-exponential functional form above and the Mg-MOF-74-Yu cluster model, for CO_2 and Mg-MOF-74. These parameters should be read in as input into our group's lattice simulation code, see `http://schmidt.chem.wisc.edu/montecarlosimulationcodes` for details.

```
lennard_jones_type 1 "1 for buckingham, 2 for lennard jones"

" parameters are listed as charge, A,B,C, polarizability
" units are A:kJ/mol,  B:A^-1,  C: KJ/mol*A^6   epsilon:KJ/mol,   sigma:A,  polarizability: A^3 "
" polarizability is defined as q^2/k, spring constant is set to .1*1.8897^3 e^2/A^3"


solute_species
atom_type_parameters  ( q, Aexch, Aelec, Aind, Adhf, Adisp, C6, C8, C10, alpha )
2
C0      0.6573800       95510.43       -27846.98       -13425.1  2065.044
        0.0     6.891E02 0.0 0.0 1.1926153
O0      -0.328690       521902.066     -163908.84      -4475.8095       -26042.04
        0.0     1.8341E03 0.0 0.0   0.9009290

solute parameters for framework cross terms  ( Aexch, Aelec, Aind, Adhf, Adisp, B, C6, C8, C10, C12 )
C0 74376.65 24130.18     12513.37          795.36
        0.0 3.4384        1147.41867     6329.41038    29659.50100    183546.714
O0 354373.13 108208.5      2544.89        -18178.7
        0.0 3.7795   867.27598     4266.54582    28761.10636  132581.301

solute dhf cross terms (check code for input format if more than one cross term)
-6124.0

solute-solute exponents ( Bii, Bij, Bjj)
3.5105206 3.6993494 3.9288490


framework_species
atom_type_parameters   ( q, Aexch, Aelec, Aind, Adhf, Adisp, B, C6, C8, C10, C12, alpha )
9
C1  -0.1639350  612892.611  229850.679   -6511.529  -60036.930
        0.000       3.438     1628.820002     6821.530007    44464.989999   193602.980000  0.0
H1   0.2637500    8538.651    1678.771    -612.739    -502.639
        0.000       3.778      129.439978      679.640001     4995.299998        0.000000  0.0
C2  -0.3191850  612892.611  229850.679   -6511.529  -60036.930
        0.000       3.438     1628.820002     6821.530007    44464.989999   193602.980000  0.0
C3   0.4964850  612892.611  229850.679   -6511.529  -60036.930
```

```
        0.000       3.438     1628.820002     6821.530007    44464.989999   193602.980000  0.0
O3  -1.0339500    3398.424    1965.168    -182.412    -178.025
        0.000       2.457     2237.635879    29956.090890   561056.184030  7451461.601923  0.0
C4   0.9468300  263600.161  112896.479     -11.681   -2837.170
        0.000       3.438      772.870024     2349.180008    27539.189998   102366.260000  0.0
O4  -0.8903225  656757.170  174054.351  -45410.640  -33954.271
        0.000       3.779     1799.560008    11576.089993    50164.639999        0.000000  0.0
Mg   1.5906500     917.037    2417.463  -12542.799       0.000
        0.000       2.834      630.723467        0.000000        0.000000        0.000000  0.0
Du   0.0000000   29176.333       0.000  142260.481       0.000
        0.000       3.973        0.000000        0.000000        0.000000        0.000000  0.0
```

5.B Simulation Parameters CO_2 Adsorption in Mg-MOF-74

Lattice simulation parameters for CO_2 adsorption in Mg-MOF-74. Of particular importance is the 'orientation_try' keyword, which is necessary to sample the specific binding geometries CO_2 adopts when binding to the open-metal site. These simulation parameters should be read in as input into our group's lattice simulation code, see `http://schmidt.chem.wisc.edu/montecarlosimulationcodes` for details.

```
Simulation Methodology
energy_decomposition yes        ! yes for our force fields, no for UFF LJ, etc.
solute_cross_parameter_set yes    ! this should be set to yes if using different solute parameters
            ! for solute-solute and solute-framework interactions as in our force fields, no otherwise
C8_10_dispersion_terms yes    ! set to yes if using C8, C10 dispersion terms as in our force fields
C12_dispersion yes
electrostatic_type pme    ! either "pme" for particle-mesh ewald, "cutoff", or "none"
lj_comb_rule ZIFFF    ! "opls" or "standard" for lj, "standard" or "ZIFFF" for bkghm

Simulation Parameters
temperature 296.0 ! temperature in Kelvin
too_close 1.8 ! reject move if molecules are within this separation in Angstroms.
            ! helpful to avoid unnecessary energy calculations and to prevent drude oscillator catastrophes
lj_bkghm 1 ! 1 for bkghm force field, 2 for lj
screen_type 1 ! screening for coulomb potential: 0 = no screening, 1 = Tang-Toennies type screening for our force fields
springconstant 0.1 ! spring constant for drude oscillators (au). set to 0.1 for our CO2/N2 force fields
thole 2.0 ! thole parameter for intra-molecular drude oscillator screening.  Set to 2.0 for our CO2/N2 force fields.
drude_simulation 1 ! set to 1 if drude-oscillators are being used, 0 otherwise
pme_grid                        100             ! size of the pme grid
alpha_sqrt                      0.6             ! alpha sqrt for the electrostatic interactions
lj_asqrt                        0.6             ! alpha sqrt for the pme dispersion
lj_cutoff                       7.5             ! cutoff for long range LJ or C6,C8,C10 dispersion interactions
ewald_cutoff                    5.0             ! cutoff for real space pme
cav_grid_a                      30
cav_grid_b                      30
cav_grid_c                      30
na_nslist                       30              ! neighbour list searching grid
nb_nslist                       30              ! neighbour list searching grid
nc_nslist                       30              ! neighbour list searching grid
orientation_try                 2000            ! max number of orientation samplings
REL_THRSH                       0.05            ! sampling threshold
ABS_THRSH                       3.0
BZ_CUTOFF                       100.0
```

6 BENCHMARK DATABASE FOR AB INITIO FORCE FIELD DEVELOPMENT

Part IV

Practical Matters

7 WORKFLOW FOR INTERMOLECULAR FORCE FIELD DEVELOPMENT

Due in part to the improvements in Chapters 3 and 4, the development protocol for Symmetry-Adapted Perturbation Theory (SAPT)-based, ab initio force fields is now fairly robust with respect to many parameterization details. Consequently, much of the workflow is now automated and requires little user input. The following sections are designed to give future users familiarity this workflow, not only as a "blackbox" tool, but also as a starting point for more complex and/or system-specific force field development. To this end, we first provide an overview of the workflow itself, and then describe the theoretical and practical details of each step in subsequent sections.

In order to gain expertise in practical force field development, new force field developers are encouraged to read through (in order) Chapters 2, 7 and 8 to obtain a conceptual understanding of the force field development process, after which they should work on developng their own force field using the semi-automated workflow (Chapter 7) and the **P**arameter **O**ptimizer for **Inter**-molecular Force Fields (POInter) software (Chapter 8). Developing a water force field makes for an excellent teaching example, however any interesting (and preferably small!) molecule will suffice.

7.1 Overview

As discussed in Chapter 2, our SAPT-based force field methodology principally requires us to parameterize the two-body interactions for a given system of interest. These two-body (i.e. dimer) interactions are completely defined by the positions and relative orientation of the two constituent monomers, and in practice we parameterize the two-body interactions based on benchmark SAPT energies for a series of gas-phase dimer configurations.[†] We are usually interested in ob-

[†]This philosophy of force field development was one of the most counter-intuitive ideas I had to learn as a grad student. Still, and regardless of whether we are ultimately interested in studying

taining transferable parameters for a new molecule or atomtype, in which case it is often easiest to model the interactions between two identical monomers (a so-called homo-monomeric dimer interaction). Still, there are reasons why it can be advantageous to instead study hetero-monomeric dimer interactions,* and the workflow described herein applies equally to studying both homo-monomeric and hetero-monomeric interactions.

Regardless of the chosen dimer of study, developing force fields for the two-body potential energy surface (PES) involves two major steps. First, we must obtain benchmark two-body energies for a series of well-chosen dimer configurations. Second, we must calculate and/or fit all force field parameters so as to completely describe a model for the two-body interaction energies. For the SAPT-based force fields described in Chapters 3 and 4, these two overarching steps lead to the following workflow:

Aside from the last step of this workflow, which will be the subject of Chapter 8, the entire force field development process has been made reasonably 'black-box', and can be carried out via a handful of input files and easy-to-use run scripts. This semi-automated workflow for SAPT-based force field development is available for download at `https://github.com/mvanvleet/workflow-for-force-fields`, and should be sufficient for most routine force field development. Installation and usage instructions are included on the website, and are also reprinted in Fig. A.1 for conveninece.

---

a homogeneous liquid or a heterogeneous supercritical phase, the best starting point for ab initio force field development is always to model all relevant gas-phase dimer interactions.

*In general, force field development based on homo-monomeric interactions involves the fewest atomtypes, and thus the fewest number of free parameters. Alternately, hetero-monomeric-based force field development can yield the best accuracy for studying systems where either transferability is difficult (see Chapter 5 for an example) or computational expense is an issue. (For instance, running SAPT calculations on a napthalene dimer may be infeasible, whereas studying napthalene-Ar interactions is easily possible.)

I) Generate benchmark two-body energies

   1) Generate a series of well-chosen dimer configurations (see Section 7.2)
   2) Calculate DFT-SAPT benchmark energies for all dimer configurations from the previous step (see Section 7.3)
   3) Optionally (depending on system size and the accuracy of DFT-SAPT for the chosen system), calculate CCSD(T) or CCSD(T)-f12 benchmark energies in order to correct the DFT-SAPT energies above (see Section 7.4)

II) Parameterize the two-body PES

   1) For each unique monomer, obtain the following monomer-specific parameters:
      i. Multipole moments, Q (see Section 7.5.2)
      ii. ISA Exponents, B (see Section 7.5.3)
      iii. Dispersion Coefficients, C_n (see Section 7.5.4)
      iv. Induced Dipole Polarizabilities, α (see Section 7.5.5)
   2) Obtain all remaining force field parameters by fitting a chosen force field functional form to the two-body benchmark energies from Step I) (see Chapter 8)

Figure 7.1: The workflow for SAPT-based force field development.

7.2 Geometry Generation

7.2.1 Guiding Principles

For any given monomer(s) of interest, the first step in the force field development process is to choose a series of optimal dimer configurations. This 'optimal' set is highly dependent on the type of force field that is being fit, and indeed the recommendations offered below are specific to the SAPT-based force fields described in Chapters 3 and 4.

In general, and as shown in Fig. 7.2, a given PES will have (qualitatively) three different regions: a repulsive wall, a minimum energy region, and an asymptotic

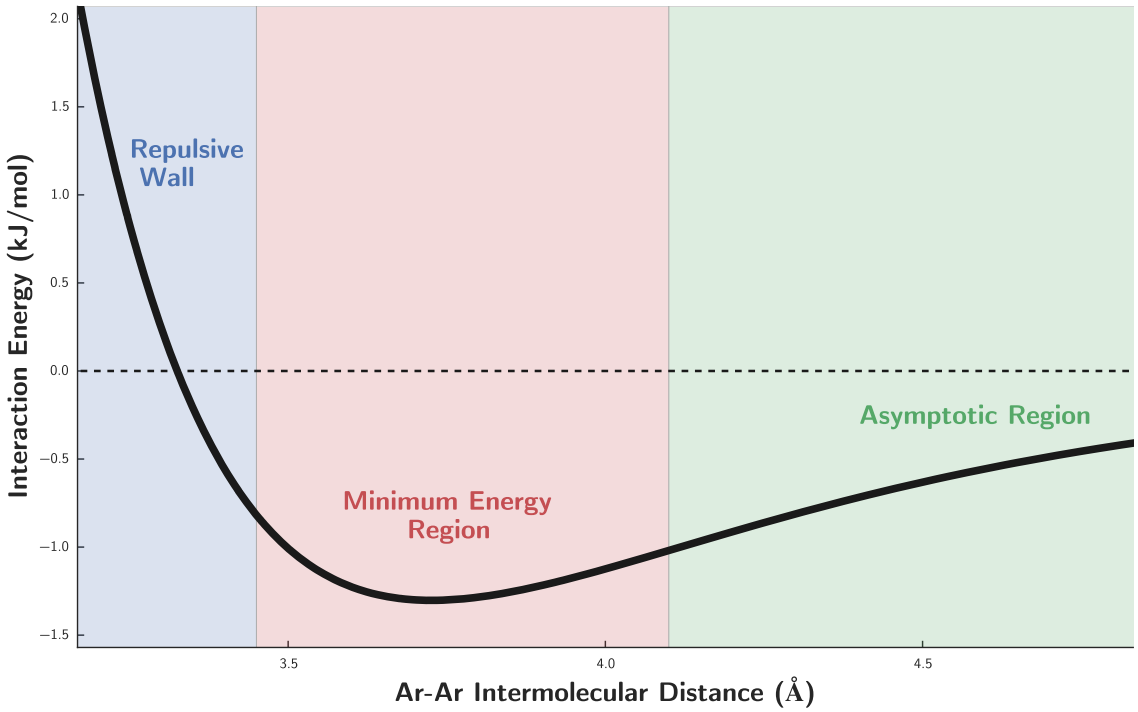

Figure 7.2: Generalized form of a PES showing the repulsive wall, minimum energy, and asymptotic regions of the argon dimer. Cutoffs between the different regions should be taken qualitatively.

region (which is often attractive, but which may be repulsive due to unfavorable electrostatic interactions). Due to the nature of the Boltzmann distribution, *routine molecular simulation will most frequently sample the minimum energy and asymptotic regions of the potential, making these portions of the PES the most important to model correctly*. Nevertheless, and as discussed in Section 7.5, the asymptotic region of the PES primarily depends on functionals forms whose parameters are calculated from monomer properties, making the dimer-based fits described in Chapter 8 relatively insensitive to inclusion of configurations in this region.* By contrast, the fitted force field parameters largely determine the shape of the repulsive wall and (to a lesser

*By contrast, other functional forms (e.g. Lennard-Jones) *do* have parameters that effect the asymptotic region, and for these force fields it would be important to include this region in the parameterization process.

extent) the minimum energy regions, and so in practice we primarily focus on including dimer configurations in these regimes.* In other words, and based on a combination of importance in molecular simulation and fit sensitivity to the specific parameters which we are directly optimizing, *the repulsive wall and especially the minimum energy regions are the most important to effectively sample in order to achieve good force field fits*.

As described below, a standard procedure for the properly sampling across the PES has been established for the Slater-ISA FF and MASTIFF force fields. Only when fitting different functional forms will the user need to reconsider the relative sampling of dimer configurations.

7.2.2 Theory

Assuming rigid monomer geometries, a dimer configuration can be completely determined (without loss of generalization) by fixing the first monomer at the origin and by placing the second monomer according to the following six variables: r, θ, and ϕ determine the position of center of mass of the second monomer, and the three-dimensional variable Ω determines the relative orientation of the monomer about its center of mass. In practice, Ω is most easily described by a quaternion approach, see Ref. 31.

For both the Slater-ISA FF and MASTIFF fits, dimer configurations are sampled psuedo-randomly using Shoemake's algorithm[32] (which ensures even sampling across the center of mass orientation) subject to some exclusion criteria. In particular, and in order to achieve representative sampling of the repulsive wall and minimum energy regions, the following dimer configurations are excluded from sampling:

1. Configurations with any atom-atom contact distance $r_{ij} \leqslant 0.8 \times (r_i^{vdw} + r_j^{vdw})$,

*Historical note: For force field functional forms which poorly model the repulsive wall (e.g. Lennard-Jones force fields or the Born-Mayer-IP FF described in Chapter 3), the force field fit quality is highly sensitive to the relative representation of repulsive and attractive dimer configurations. (Including both too few or too many repulsive configurations can be problematic). Only with the advent of Slater-ISA FF and MASTIFF has the fit quality become strictly improved by including repulsive configurations.

where r_{ij} is the contact distance and r^{vdw} is the tabulated van der Waals radius for a given element

2. Configurations with all atom-atom contact distance $r_{ij} \geqslant 1.3 \times (r_i^{vdw} + r_j^{vdw})$

7.2.3 Practicals

In practice, generation of the dimer configurations is fairly straightforward. The required input files – `dimer_info.dat`, `generate_grid_settings.inp`, and `<mona>_<monb>.inp` – are listed in Listings 7.1 to 7.3 and using the pyridine dimer as an example. Each input file may need to be modified for the dimer under consideration, and comments within each input file explain any necessary system-specific changes.

Once these input files have been modified, the geometry generation process can be carried out very simply from the main force field fitting directory by executing the command

```
./scripts/make_geometries.sh
```

7.3 SAPT Benchmarks

After geometry generation, the next step is to run benchmark DFT-SAPT calculations on all dimer configurations. For a detailed analysis of SAPT, and DFT-SAPT in particular, the reader is referred to Refs. 24, 33, 34. DFT-SAPT calculations can be performed in a fairly black-box manner, though the points are worth mention:

1. For best accuracy, and as described in Ref. 29, the monomer Density Functional Theory (DFT) calculations need to be asymptotically-corrected (AC) for best accuracy. This asymptotic correction is computed as the difference between the HOMO and the vertical ionization potential for each monomer, and is calculated automatically by running the command

```
./scripts/submit_ip_calcs.py
```

(The calculation takes only a few minutes for small molecules, but may take longer for larger systems.) Importantly, the HOMO calculation should be computed in the same basis as the DFT-SAPT calculations themselves.

2. Accurate SAPT dispersion energies generally require use of midbond functions, as described in Ref. 29. Locations for the midbond functions can be specified in the `dimer_info.dat` file. For most small molecules (such as those described in Chapter 3), it is often sufficient to place a single midbond at the midpoint between each monomer's center of mass. For larger molecules, additional midbonds (especially ones near close-contact interaction sites) may be required.

3. The included workflow assumes an aVTZ+m basis set (where the +m represents the midbond functions). This is generally sufficiently accurate for most systems, though an aVTZ+m basis set should be used when possible to ensure convergence of the DFT-SAPT dispersion energies.

Once the appropriate midbond functions have been added to the `dimer_info.dat` input file, and the AC calculations have finished, the DFT-SAPT input files can be generated by executing the command

```
./scripts/make_sapt_ifiles.py
```

The resulting input files can then be run using the Molpro software, either in serial or in parallel. *Care should be taken to ensure that multiple calculations do not end up on the same compute note, as this can often result in i/o caching issues and reduced computational efficiency.*

7.4 CCSD(T) Calculations

When affordable, CCSD(T) calculations should be run on (at least a subset of) the dimer configurations, both in order to benchmark the DFT-SAPT energies and to provide a δCCSD(T) correction for later fitting of the SAPT potential. Recently, an explicitly-correlated CCSD(T)-f12 method has been proposed, which for practical

purposes is identical to CCSD(T) but with faster basis set convergence.[35] Usually CCSD(T)-f12a/aVTZ+m is an excellent approximation of the CCSD(T)/CBS limit. The input files for CCSD(T)-f12/aVTZ+m calculations can be set up by executing the command

```
./scripts/make_ccsdt_ifiles.py
```

and by running each input file using the Molpro software package.

7.5 Monomer-Based Parameterization

7.5.1 The CamCASP software

CamCASP is a collection of scripts and programs useful for (among other things) the calculation of distributed multipoles and polarizabilities.[36] Of particular theoretical importance is the distribution method, as this determines how the various molecular properties of interest should be mapped onto corresponding atom-in-molecule properties. Currently, two main distribution (or 'charge partitioning') schemes are available in CamCASP: Distributed Multipole Analysis (DMA)[37] and Iterated Stockholder Atoms (ISA).[38] The theory behind the ISA procedure has already been detailed in Chapter 2, and monomer property calculations using DMA are described in Ref. 24, 37, 39. In general, and where available, ISA-based properties are to be preferred, and we recommend an ISA-based parameterization scheme for obtaining multipoles and atom-in-molecule exponents. A DMA-based method is currently required for obtaining dispersion coefficients and static polarizabilities, though ISA-based strategies for these properties are under active development, and a workflow for obtaining ISA-based dispersion coefficients are discussed below. A complete overview of available properties and distribution schemes, along with relevant references, are listed in Table 7.1.

Property	Parameterization Scheme	
	ISA	DMA
Multipoles	Section 7.5.2 Ref. 38	– Ref. 24, 37
Exponents	Section 7.5.3 Ref. 40	–
Polarizabilities	–	Section 7.5.5 Ref. 23
Dispersion Coefficients	Section 7.5.4 –	Section 7.5.4 Ref. 23

Table 7.1: Overview of ISA- and DMA-based methods for obtaining distributed monomer properties. Details for each monomer parameterization are given in the listed section and/or reference.

7.5.2 Multipoles

Overview

ISA-based multipoles are described in detail in Ref. 38, and can be calculated using the CamCASP software. To set-up the ISA calculations, execute the command

```
./scripts/make_isa_files.py
```

which creates the necessary ISA files for calculating both distributed multipoles and exponents (see Section 7.5.3). After running these calculations (a process which may require several hours, depending on the molecule), the multipoles can be extracted simply by running

```
./scripts/workup_isa_charges.py
```

This work-up script produces several output files,

- `<monomer>_ISA_L4.mom`
- `<monomer>_ISA_L2.mom`

- `<monomer>_ISA_L0.mom`

which correspond to multipole moments for various long-range electrostatic models. Using Stone's notation,[2] the Lx notation refers to the highest order of multipole moments (L0 = point charges, L1 = dipoles, L2 = quadrupoles, etc.) included in the model. The L4 model is output by the CamCASP software package, and the L2 and L0 models are generate by rank-truncation (that is, neglect) of the higher-order multipole moments. For most routine force field development, the L2 model is preferred, however below we discuss situations in which different electrostatic models may be desirable.

Advanced Multipole Parameterization Options

For many molecules, and for the purposes of obtaining sub- kJ/mol accuracy force fields, it is often important to model the long-range electrostatics using ISA-based multipoles truncated to quadrupolar (i.e. 'rank 2' or L2)[2] contributions. Nevertheless, due to computational and/or software limitations, there may be practical cases where it becomes advantageous to exclude higher-order multipole moments.[41] In these cases, two additional types of long-range electrostatic models are possible. For reasonably isotropic molecules, one option is to further truncate the ISA multipoles to point charge contributions, yielding a so-called 'atom-centered point charge model'. For more anisotropic functional groups, such as those described in Ref. 42, an atom-centered point charge model can be insufficiently accurate, making it necessary to model the long-range electrostatics with additional 'off-center' point charges. Given a well-chosen set of off-site charges, an off-site point charge model usually can reasonably reproduce the effects of the neglected higher-order multipole moments.[43] Locations for the off-center charges are often manually tuned or optimized in a system-specific manner, though some recent work suggests the possibility of using non-empirical methods to directly calculate/optimize positions for the extra-atom sites.[44,45]

For an atom-centered point charge model, the output of the `workup_isa_charges.py` script automatically provides the required rank-truncated multipole file (listed as

<monomer>_ISA_L0.mom in the isa/ sub-directory). Note that, because the <monomer>_ISA_L0.mom file is given as a simple rank-truncation of the more complete <monomer>_ISA_L2.mom multipoles, the L0 moments (that is, point charges) are identical between the two files.

For developing rank-transformed point charge models, Ferenczy et al. has programmed a method for calculating electrostatic potential-fitted charges, which can be thought of as a 'rank transformation' procedure. The author's MULFIT program can be downloaded online at http://www-stone.ch.cam.ac.uk/pub/gdma/index.php, and documentation for the program is found in the documentation/ subdirectory of the workflow. Assuming the mulfit executable is in your $PATH, the rank transformation can be performed using the following steps:

```
cp templates/mulfit.inp isa/<monomer>/OUT/
cd isa/<monomer>/OUT/
mulfit < mulfit.inp
```

where the default mulfit.inp file is set to take in the L4 rank multipoles and rank-transform them to an L0 model. In this case, note that the L0 moments between the rank-transformed and rank-truncated moments will *not* be identical, and testing is required to ascertain which moments yield optimal force field parameters.

The MULFIT program can additionally be used to develop off-site point charge models. In this case, the input multipole file (default ISA_L4.mom) should be edited to include the additional sites, and an example of the required syntax is given in documentation/examples/ISA_L4_offsites.mom using a 4-site water model as an example. Note that the MULFIT program does not help optimize the position(s) of the off-site charge(s), and thus the task of choosing the number and position(s) of the off-site(s) is left to the user.

After fitting multipole parameters with the MULFIT program, the program output gives two indications of fit quality. First, the agreement between the total reference and fitted multipoles moments is listed, and this should be taken as a primary indication of multipole quality. Second, the program gives a 'Goodness of fit' parameter, expressed as an energy. While difficult to interpret in an absolute sense, in comparing different rank-transformed models we have generally found

that models with lower 'Goodness of fit' parameters yield better force field fits.

7.5.3 ISA Exponents

As described in Chapters 2 and 3, the ISA procedure produces a set of distributed atom-in-molecule (AIM) electron densities. The orientational average of each of these AIM densities, or 'shape-functions', are spherically-symmetric functions that describe the radial decay of the AIM density.[38] As described in Chapter 3, and using the algorithm detailed in Section 7.B, the shape-functions can be fit to a Slater-type function in order to yield an isotropic, exponentially-decaying model for the ISA densities. Importantly, the Slater-exponents in this density model directly yield the exponents necessary to describe short-range effects (such as exchange-repulsion and charge penetration) in the two-body force field (see **??**).

Assuming the ISA calculations have already been run to obtain multipole moments (see previous section), the ISA exponents can be obtained very simply by running the command

```
./scripts/workup_isa_exponents.py
```

The resulting exponents are given in the file `isa/<monomer>.exp`, which uses a file format recognized by the POInter pre-prossessing scripts (see Chapter 8).

7.5.4 Dispersion Coefficients

Theory

Dispersion coefficients can also be determined from distributed molecular (that is, AIM) property calculations using either an ISA- or DMA-based approach. The method for obtaining distributed dispersion coefficients has been described in detail elsewhere for an assortment of DMA-based approaches,[2,12,23,24,47,48] and Ref. 24 in particular provides a useful summary of the different equations and molecular properties that are needed to derive the types of dispersion models used in Chapters 3 and 4. In brief, AIM dispersion energies can be obtained by integrating over distributed frequency-dependent polarizabilities for each monomer. Under

the simplifying assumption that we can treat these polarizabilities as isotropic, the dispersion energy expression is given by

$$E_{disp}^{ab} \approx -\frac{C_6^{ab}}{r_{ab}^6} - \frac{C_8^{ab}}{r_{ab}^8} - \dots \tag{7.1}$$

for each atom pair, where

$$C_6^{ab} = \frac{3}{\pi}\int_0^\infty \bar{\alpha}_1^a(i\omega)\bar{\alpha}_1^b(i\omega)d\omega, \tag{7.2}$$

$$C_8^{ab} = \frac{15}{2\pi}\int_0^\infty \bar{\alpha}_1^a(i\omega)\bar{\alpha}_2^b(i\omega) + \bar{\alpha}_2^a(i\omega)\bar{\alpha}_1^b(i\omega)d\omega, \tag{7.3}$$

and the higher order terms are defined analagously. C_n^{ab} are the atom-atom dispersion coefficients, and $\bar{\alpha}_l^a$ are the rank l, isotropic, AIM frequency-dependent polarizabilities. The formalisms in Eqs. (7.2) and (7.3) can be somewhat involved, but for our purposes the important take-away is the understanding that the dispersion coefficients can be entirely determined by calculating the frequency-dependent polarizabilities for each atom in its molecular environment.

Although it is straightforward to calculate *molecular* frequency-dependent polarizabilities, a central difficulty in obtaining transferable dispersion coefficients is that, in order to evaluate Eqs. (7.2) and (7.3), we must have some physically-meaningful method for calculating *atom-in-molecule* polarizabilities. Many distribution strategies exist in the literature, and here we focus on two such techniques. First, and as we have used in Chapters 3 and 4, one can utilize a DMA-based approach to partition the polarizabilities into AIM contributions. In this case, and due to deficiencies in the DMA partitioning scheme, the resulting atomic polarizabilities are not always positive-definite and monotonically-decaying, and this unphysical behavior can lead to a breakdown in transferable parameterization.[47] To correct for this undesirable behavior, McDaniel and Schmidt have proposed a constrained fitting procedure whereby atomic polarizabilities can be optimized in an iterative fashion,

thereby generating transferable atomic polarizabilities at the expense of requiring a fairly large training set for each unparameterized atomtype (see Section 7.5.4 for details).

As an alternative to the above iterative polarization partitioning scheme, recently Misquitta has developed an ISA-based partitioning scheme to extract the atomic frequency-dependent polarizabilities. While this approach requires further testing, and is not yet published, the resulting 'ISA-pol' method appears to lead to a more physically-meaningful partitioning of the molecular polarizabilities. For practical purposes, this more physical partitioning enables us to determine transferable dispersion coefficients without resorting to large training sets. Formalisms and technical details related to ISA-pol are the subject of Section 7.5.4, and a comparison between the two methods for obtaining dispersion coefficients is given in Section 7.5.4. Finally, each method for obtaining dispersion coefficients requires a small amount of post-processing, and this is discussed in Section 7.5.4.

Iterative-DMA-pol

As described in Ref. 24, the iterative-DMA-pol (iDMA-pol) method of McDaniel and Schmidt performs a constrained optimization of atomtype-specific frequency dependent polarizabilities by fitting all polarizabilities to reproduce the so-called 'point-to-point response', α_{PQ}. This point-to-point response is a molecular quantity that describes the change in electrostatic potential at point P due to an induced change in the electron density of a molecule caused by a point charge perturbation q_Q at point Q. For an isotropic polarizability model,

$$\alpha_{PQ} = -q_Q \sum_{a,lm} T^{Pa}_{0,lm} \bar{\alpha}^a_l T^{aQ}_{lm,0} \tag{7.4}$$

where the T are the spherical harmonic interaction functions described above and in Ref. 2. Aside from the isotropic polarizabilities $\bar{\alpha}^a_l$, all quantities in Eq. (7.4) are directly calculated in CamCASP, enabling us to fit the isotropic polarizabilities based on a CamCASP properties calculation (see Appendix A of Ref. 24 for details).

Using the iDMA-pol method in the Workflow has two software dependencies:

1. The iDMA-pol fiting program itself, which can be downloaded at `https://github.com/mvanvleet/p2p-fitting`. Three executables (`main_dispersion`, `main_drude`, and `localize.sh`) need to be added to your bash `$PATH` for the scripts listed in this section to work properly.

2. CamCASP, which can be downloaded from `http://www-stone.ch.cam.ac.uk/programs/camcasp.html`. CamCASP also requires several environment variables to be added to your bash `$PATH`, and some of these environment variables are also used by the iDMA-pol fitting program.

and requires two additional input files:

1. `input/<monomer>.atomtypes`: The iDMA-pol fitting program performs a constrained optimization whereby the $\bar{\alpha}_l^q$ are set to be identical for atoms with the same atomtype. Consequently, the `<monomer>.atomtypes` input file is required to specify the atomtypes in each monomer. This .atomtypes file has the same format as an .xyz file, with the exception that the element names for each atom are replaced with a user-defined atomtype. See Listing 7.4 for an example with pyridine.

2. `templates/dispersion_base_constraints.index`: As described below, with iDMA-pol it is usually advisable to only fit one or two atomtype polarizabilities at a time, with the remaining atomtype polarizabilities read in as hard constraints. The `dispersion_base_constraints.index` file lists these hard constraints in a block format,

```
CT
1
 7.14483224 7.11095841 6.87452508 6.19718464 4.87589777
 3.17818610 1.56461102 0.51670933 0.09175313 0.00367230
2
 20.26394042 20.00584110 17.66562710 14.33668329 12.03179893
 11.49156262 7.86254302 3.10936998 0.53746459 0.01774391
3
 77.37303638 73.13014787 24.68682297 −13.48390193 0.40172836
 29.76747226 34.31668916 17.88515654 3.13260459 0.10137127
```

which lists each constrained atomtype along with 10 frequency-dependent polarizabilities for each polarizability rank (1-3). (CamCASP uses numerical integration to solve Eq. (7.2), and the 10 polarizabilities per rank correspond to the frequencies CamCASP needs to perform the numerical quadrature. See the CamCASP user manual for details.) Each polarizability block should be separated by a blank line, and the atomtypes listed in the .index file *must* match those in the .atomtypes file for any hard constraints to be applied. Previously-fit atomtype polarizabilities from Ref. 23 are already included in `dispersion_base_constraints.index` so as to minimize the number of hard constraints that the user will need to add manually, and these hard constraints should be used whenever possible.

Once all required input files have been created, and assuming the IP calculations from Section 7.3 have already been performed, the CamCASP calculations necessary to run the iDMA-pol program can be performed by executing the command

```
./scripts/make_dmapol_files.py
```

and running the resulting input files through the CamCASP software (a process which can take several hours). Once the CamCASP calculations finish, dispersion coefficients can be obtained by running the following work-up script:

```
./scripts/workup_dispersion_files.sh
```

The resulting dispersion coefficients will be listed in the `dispersion/<monomer>.cncoeffs` output file.

When generating dispersion coefficients using iDMA-pol, the following sanity-checks should always be performed:

1. The `<monomer>_fit_dispersion.out` file lists the number and names of unconstrained atomtypes. Ensure that the number and type of unconstrained atomtypes match your expectations, and that the number of fit atomtypes is kept relatively small (1-2 max). If you need to fit multiple atomtypes simultaneously, or you obtain unphysical disperion coefficients (see next point),

you'll likely need to utilize the iterative fitting algorithm outlined in Ref. 23 or obtain dispersion coefficients from an ISA-based scheme (Section 7.5.4).*

2. Dispersion coefficients should always be positive. Any negative dispersion coefficients are likely a sign of unphysical atomic polarizabilities (see next point).

3. Phsyically-speaking, the atomic polarizabilities at each rank should be positive definite, and monotomically-decreasing.[2?] Unphysical behavior (especially at rank 3) is sometimes unavoidable, but often indicates poor fit quality and can lead to inaccurate and/or non-transferable dispersion coefficients. Always check the output `.casimir` files for the physicality (positive-definiteness and monatomic-decrease) of the frequency-dependent polarizabilities for each atomtype and each rank.

Finally, given a set of physical atomic polarizabilities and dispersion coefficients, dispersion coefficients from the iDMA-pol method can be worked-up using the post-processing scripts described in Section 7.5.4.

ISA-pol

Theory Rather than iteratively fitting polarizabilities to reproduce the point-to-point response, with ISA it is possible to compute the atomic polarizabilities directly. First, note that the frequency-dependent, molecular polarizabilities are given by the following formula:

$$\alpha_{lm,l'm'}(\omega) = \int\int \hat{Q}_{lm}(\mathbf{r})\alpha(\mathbf{r},\mathbf{r'}|\omega)\hat{Q}_{l'm'}(\mathbf{r'})d\mathbf{r}d\mathbf{r'} \tag{7.5}$$

Here $\hat{Q}$ are the regular spherical harmonic operators (defined in Appendix A of Ref. 2) of rank l and order m, and $\alpha(\mathbf{r},\mathbf{r'}|\omega)$ is the frequency-dependent density susceptibility (FDDS), or charge density susceptibility, which measures the change

*Scripts to perform the iterative iDMA-pol fitting algorithm can be made available upon request.

in charge density at $\mathbf{r}'$ that results from a delta-function change in the electric potential at point $\mathbf{r}$. From **??**, we have that

$$1 = \sum_a \left(\frac{\bar{w}^a(\mathbf{r})}{\sum_m \bar{w}^m(\mathbf{r})} \right) = \sum_a \bar{p}_a(\mathbf{r}), \tag{7.6}$$

where the bars indicate that we have normalized the atom-in-molecule densities and weight functions. Substituting this equation into Eq. (7.5), we arrive at an ISA-based definition of the AIM polarizabilities:

$$\begin{aligned} \alpha_{lm,l'm'}(\omega) &= \int\int \hat{Q}_{lm}(\mathbf{r}) \alpha(\mathbf{r},\mathbf{r}'|\omega) \hat{Q}_{l'm'}(\mathbf{r}') d\mathbf{r} d\mathbf{r}' \\ &= \sum_a \sum_b \int\int \hat{Q}_{lm}(\mathbf{r}) p_a(\mathbf{r}) \alpha(\mathbf{r},\mathbf{r}'|\omega) p_b(\mathbf{r}') \hat{Q}_{l'm'}(\mathbf{r}') d\mathbf{r} d\mathbf{r}' \\ &\equiv \sum_a \sum_b \alpha^{ab}_{lm,l'm'}(\omega) \end{aligned} \tag{7.7}$$

While this formula bears similarity to DMA-based polarization approaches,[47,48] the advantage of Eq. (7.7) is that the AIM polarizabilities are defined in a physically-meaningful and transferable manner. Consequently, with little refinement these ISA-based polarizabilities (ISA-pol) can be used to directly obtain transferable dispersion coefficients for individual atom-in-molecule, all without recourse to the iterative fitting process required in Section 7.5.4.

Practicals The ISA-pol method has been completely implemented as of CamCASP-6.0, though the input scripts are (as of this writing) still in beta. Consult the CamCASP user manual for up-to-date details and required input files.

Method Comparison

Preliminary results for the ISA-pol method, tested on the 91 dimer test set, appear to be of similar accuracy compared to the iDMA-pol method, though both methods appear to have their own strengths and weaknesses when it comes to obtaining dispersion coefficients for different atomtypes. A comparison between the two

different methods is given in Table 7.2. Overall, ISA-pol appears to give more physically-meaningful atomic polarizabilities, whereas an isotropic iDMA-pol description is (for anisotropic systems) sometimes a better 'effectively anisotropic' model.*

Dispersion Coefficient Post-processing

Regardless of which distribution method is used, some post-processing is needed to transform the ISA-pol/iDMA-pol coefficients into optimal dispersion force field parameters. In particular, while the DFT-SAPT energies from Molpro and CamCASP should agree, in practice the different software packages use different kernels (ALDA+LHF and ALDA+CHF, respectively) to calculate the linear response functions. Consequently, this means that the dispersion coefficients calculated in CamCASP are intended to reproduce the CamCASP-calculated DFT-SAPT dispersion energies, but may only be approximately accurate for Molpro-calculated DFT-SAPT dispersion energies.† In practice, the CamCASP-calculated dispersion coefficients slightly underestimate the Molpro dispersion energies, and the coefficients need to be scaled (usually by a factor of 1.03-1.10, depending on the atomtype) to reproduce the Molpro energies. This scaling can be carried out by executing the command

```
./scripts/get_scaled_dispersion.py <scale_factor>
```

where `<scale_factor>` is chosen to reproduce the asymptotic Molpro DFT-SAPT energies (see Chapter 8). This choice may require some testing, but 1.10 is usually a good default. The above script outputs files `dispersion/<monomer>.disp`, which can be used as input to the POInter program discussed in Chapter 8.

* A main difference between the iDMA-pol and ISA-pol coefficients is that iDMA-pol fits more strongly to the p2p file, whereas ISA-pol coefficients are set to the values calculated as in Section 7.5.4. Consequently, iDMA-pol is able to perform better as an 'effectively anisotropic' model. In principle, changing the defaults in CamCASP to use weight type 4 (which uses dipole-dipole terms as anchors, but completely fits higher ranking terms and thus fits the p2p better) or 3 (uses all terms as anchors) and a weight coefficient of 1e-5 (rather than 1e-3) should yield dispersion coefficients more similar to iDMA-pol, though this idea requires further testing.

† Additional reasons for discrepancies between CamCASP and MOLPRO dispersion coefficients include the following:

iDMA-pol	ISA-pol
Ease of Parameterization	
• For systems with 1-2 unparameterized atomtypes, little cost to parameterize new atomtypes • For systems requiring dispersion coefficients for several unparameterized atomtypes, requires a library of systems containing these atomtypes, and an iterative procedure to fit the new atomtypes.	• Straightforward for all molecules, regardless of number of unparameterized atomtypes
Physicality of the Distributed Polarizabilities	
• Polarizabilities tend to be positive-definite and monotonically-decaying at low rank, but not always at rank 3 • Physicality highly-dependent on quality of previously parameterized atomtypes	• With few exceptions, polarizabilities are positive-definite and monotonically-decaying at all ranks
Accuracy of the Dispersion Coefficients	
• Good to excellent accuracy for atomtypes which have been fit to a reproduce large library of molecular systems • Fair accuracy for certain atomtypes (such as chlorine or bromine) not parameterized to an extensive library • For anisotropic systems (such as CO_2), tends to give a better isotropic description than ISA-pol – we hypothesize that this is a result of directly fitting the point-to-point response, leading to an 'effectively-anisotropic' model	• Good to very good accuracy for all tested systems, regardless of what atomtypes are represented • Isotropic dispersion coefficients tend to give worse accuracy for anisotropic systems compared to iDMA-pol, whereas anisotropic dispersion models (see Chapter 4 based on ISA-pol are of similar accuracy to the iDMA-pol method

Table 7.2: Comparison between the iDMA-pol and ISA-pol methods.

7.5.5 Polarization Charges

Theory

In addition to frequency-dependent polarizabilities, some of the same techniques described in Section 7.5.4 can be applied to obtain the drude oscillator charges that get used in modeling the induction energy. Though in principle ISA-based polarizabilities could be used, this technique has not yet been developed. Instead, an iDMA-pol-type procedure can be used to extract the necessary polarization parameters. The algorithms used to perform this procedure are described in Appendix A of Ref. 24. Due to the reduced number of coefficients that need to be fit, this optimization is generally more robust, and leads to more transferable dispersion parameters, than the algorithms described in Section 7.5.4.

Practicals

The drude oscillator fitting code has the same dependencies and input files as iDMA-pol, with the exception that the `dispersion_base_constraints.index` file is replaced with the following constraint file:

1. `drude_base_constraints.index`: As with iDMA-pol, it is usually advisable to only fit a few atomtype static polarizabilities at a time, with the remaining atomtype polarizabilities read in as hard constraints. The `drude_base_constraints.index` file lists these hard constraints in a block format,

1. For PBE calculations, CamCASP uses ALDA with PW91c correlation, whereas Molpro uses VWN

2. CamCASP writes kernels completely in the auxiliary basis set, whereas Molpro writes the kernel in a variety of basis sets

```
C
1
 0.0

N
1
 -11.7529643

H
1
 -1.254
```

which lists each constrained atomtype along with the rank 1 static polarizabilities, separated by a blank line. Unlike with the generation of dispersion coefficients, an initial guess must be given for *all* atomtypes in the `<monomer>.atomtypes` input file. The format for the `drude_base_constraints.index` is such that positive polarizabilities correspond to these initial guesses, whereas zero or negative entries for the polarizabilities indicate that the atomtype should be treated as a hard constraint. Previously-fit atomtype polarizabilities from Ref. 23 are already included in `drude_base_constraints.index` so as to minimize the number of hard constraints that the user will need to add manually, and these hard constraints should be used whenever possible.

Assuming that the iDMA-pol calculations have already been run in CamCASP, the drude oscillator coefficients can be obtained simply by executing

```
./scripts/workup_drude_files.sh
```

As with the dispersion coefficients, care should be taken to ensure that the resulting drude oscillator charges are physically-meaningful (i.e. negative).

7.6 Dimer-Based Parameterization

Refer to POInter Code section

7.A Input Scripts

In total, the workflow for force field development requires four input files, as follows:

Listing 7.1: generate_grid_settings.inp

```
# Generate Grid Settings file. Version 04.28.15
#
# General Scan Parameters:
n_points         1000  # Number of grid points (.xyz files) to output
geometry_file    pyridine_pyridine.inp #name of geometry file
output_name      pyridine_pyridine        #output file base name

# Hard Sphere cutoff parameters:
#
# Parameters below are used to define minimum and maximum acceptable distances
# for neighbor-neighbor interactions.  'cutoff_type' can either be set to
# 'absolute' or 'vdw'. In the former case, the hard sphere cutoff will be set
# to the absolute distances (in Angstroms) given by cutoff_min and cutoff_max,
# respectively. In the latter case, the hard sphere cutoff will be set to a
# fraction of the Van der Waals distance between two atoms.
cutoff_type      vdw   # either vdw or absolute
cutoff_min          0.8    # a positive float (ex. 0.8 for vdw or 2.0 for absolute)
cutoff_max          1.3   # a positive float (ex. 1.2 for vdw or 6.0 for absolute)

# The following are parameters defining the centers of monomer's a and b as well as the
    scan
# vector.
#
# The 'center' of each monomer is defined by default to be each
# monomer's center of mass, but can also be set to be either the center of an
# atom or a point in 3-space (relative to monomer coordinates given in input
# geometry file).
mona_origin_type  1   # choose 0 for center of mass (COM), 1 for atom#, and 2 for a
    specific point
mona_origin       6     # (either 'COM', point x,y,z , or atom# in monomer (indexing
    starts at 1), depending on choice of mona_origin_type above)
monb_origin_type  1   # choose 0 for COM, 1 for atom#, and 2 for a specific point
monb_origin       6    # (either 'COM', point x,y,z , or atom# in monomer (indexing
    starts at 1), depending on choice of mona_origin_type above)

# The scan vector should be a vector (given relative to the coordinates in
# monomer a) that defines the direction of internuclear seperation between the
# two monomers. It can either be given as a 3-membered list or by listing two
# monomer indices (scan vector will point from atom1 to atom2, indexing starts at 1).
```

```
scan_vector_type  0  # choose 0 for monomer indices, 1 for a specific point
scan_vector    9,6   # Give either as a 2 (if scan_vector_type==0) or a 3 (if
    scan_vector_type==1) membered,
                     # comma seperated list without spaces, i.e. '1.0,2.7,4.2' (no
                         quotes)

# Set bounds on moving the center of monomer b relative to the center of
# monomer a. min/max_r refers to the distance between the centers, while theta
# and phi correspond to the azimuthal and polar angles, respectively, of
# rotation about the vector scan_vector (given above).
#
# Give min/max angles as either integers/floats in terms of pi (i.e. setting
# 'max_theta 2' (no quotes) will yield  max_theta=2pi).
min_r             2.0
max_r             8.0
min_theta         0
max_theta         2
min_phi           0
max_phi           1
```

Listing 7.2: dimer_info.dat

```
##########################
# DIMER INFORMATION FILE #
##########################

# String names for monomers A and B:
# ----------------------------------
MonA_Name         pyridine
MonB_Name         pyridine

# Charges for monomers A and B:
# -----------------------------
MonA_Charge       0
MonB_Charge       0

# Midbond position(s); two integers indicating atom indices (indexed from 1)
# on monomers A and B, respectively, between which to place the midbond site.
# In lieu of an integer, COM can also be used to indicate the center of mass
# of the monomer.
# Multiple arguments can be given to produce multiple midbond functions.
# ---------------------------------------------------------------------------
midbond     com    com
```

Listing 7.3: pyridine_pyridine.inp

```
Pyridine Dimer; Optimzed with PBE0/cc-pVTZ Gaussian03 by AJ Misquitta
11
 H          -2.050322     1.274414     0.000000
 H          -2.147113    -1.203259     0.000000
 H           0.000000    -2.487558     0.000000
 H           2.147113    -1.203259     0.000000
 H           2.050322     1.274414     0.000000
 N           0.000000     1.382844     0.000000
 C          -1.134410     0.690452     0.000000
 C          -1.190513    -0.695795     0.000000
 C           0.000000    -1.403912     0.000000
 C           1.190513    -0.695795     0.000000
 C           1.134410     0.690452     0.000000
11
 H          -2.050322     1.274414     0.000000
 H          -2.147113    -1.203259     0.000000
 H           0.000000    -2.487558     0.000000
 H           2.147113    -1.203259     0.000000
 H           2.050322     1.274414     0.000000
 N           0.000000     1.382844     0.000000
 C          -1.134410     0.690452     0.000000
 C          -1.190513    -0.695795     0.000000
 C           0.000000    -1.403912     0.000000
 C           1.190513    -0.695795     0.000000
 C           1.134410     0.690452     0.000000
```

Listing 7.4: pyridine.atomtypes

```
Pyridine Dimer; Optimzed with PBE0/cc-pVTZ Gaussian03 by AJ Misquitta
11
 H          -2.050322     1.274414     0.000000
 H          -2.147113    -1.203259     0.000000
 H           0.000000    -2.487558     0.000000
 H           2.147113    -1.203259     0.000000
 H           2.050322     1.274414     0.000000
 N           0.000000     1.382844     0.000000
 C          -1.134410     0.690452     0.000000
 C          -1.190513    -0.695795     0.000000
 C           0.000000    -1.403912     0.000000
 C           1.190513    -0.695795     0.000000
 C           1.134410     0.690452     0.000000
11
 H          -2.050322     1.274414     0.000000
 H          -2.147113    -1.203259     0.000000
 H           0.000000    -2.487558     0.000000
 H           2.147113    -1.203259     0.000000
 H           2.050322     1.274414     0.000000
```

N	0.000000	1.382844	0.000000
C	−1.134410	0.690452	0.000000
C	−1.190513	−0.695795	0.000000
C	0.000000	−1.403912	0.000000
C	1.190513	−0.695795	0.000000
C	1.134410	0.690452	0.000000

7.B Extrapolation Algorithm for ISA Exponents

Unphysical asymptotic charge density decays occasionally arise in the ISA procedure due to basis set incompleteness and numerical instabilities. These unphysical decays can skew optimization of ISA-based exponents, B_i^{ISA}, and need to be corrected. Generally speaking, there exists some range of distances in the valence region that *does* exhibit the expected exponential decay; we extrapolate the decay from this intermediate region to describe the asymptotic region using the following algorithm:

1. Take the log of each atomic density (henceforth logdens) to linearize the asymptotic density.

2. Compute the 2^{nd} derivative of logdens. This can be done analytically, as the ISA procedure outputs an analytical expression (in terms of Gaussian basis functions) for the atomic density.

3. Determine the 'intermediate region' of exponential decay by locating the largest range where the 2^{nd} derivative of logdens is zero to within a fixed tolerance. Here we utilize a tolerance of 0.3 a.u. (absolute cutoff) or 190% of the smallest exponent in the Gaussian basis set (relative cutoff), whichever is smaller. The latter cutoff accounts for the eventual asymptotic Gaussian-type decay dictated by the smallest ζ in the ISA basis. The endpoints of this intermediate region are denoted r1 and r2, respectively.

4. Calculate the slope m and intercept b for the line defined by r1, r2, and their respective values of logdens.

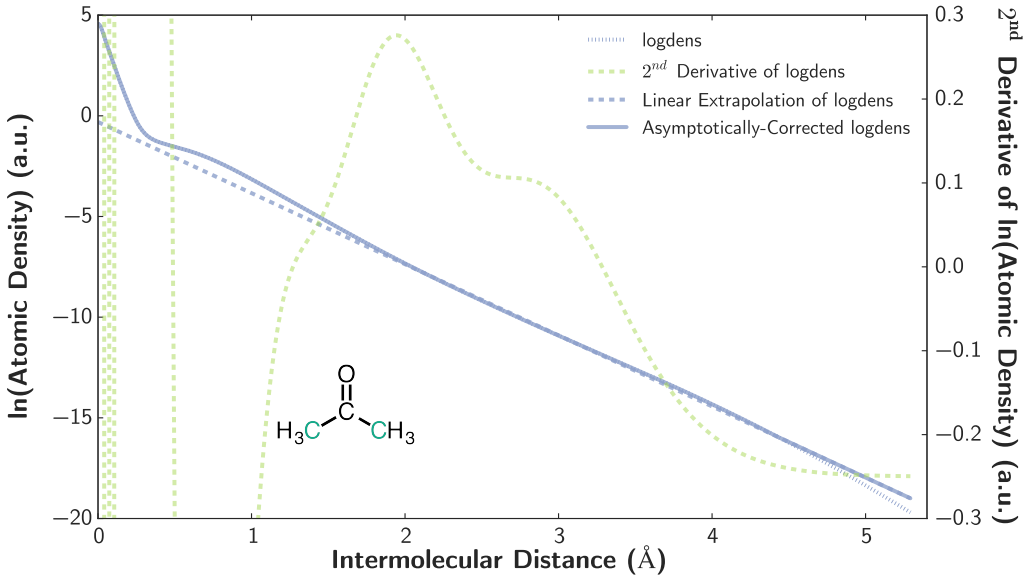

Figure 7.3: Linear extrapolation algorithm for the methyl carbon in acetone. Depicted are (in legend order) Steps 1, 2, 4, and 5 in the extrapolation algorithm. Note that some portions of the 2^{nd} derivative extend off the graph; also note that most of logdens is located underneath the asymptotically-corrected curve.

5. Replace all values of logdens after r2 with $\mathtt{m}r + \mathtt{b}$. The resulting atomic density is labeled in the main text as 'Asymptotically-corrected ISA densities'.

A visual of these steps is shown in 7.3.

8 POINTER: A PROGRAM FOR INTERMOLECULAR FORCE FIELD OPTIMIZATION

8.1 Overview

8.2 Documentation

8.3 Examples

Part V

Conclusions and Future Work

9 FUTURE WORK

10 CONCLUSIONS

Part VI

Codes

A FORCE FIELD DEVELOPMENT WORKFLOW

Purpose

Derive a first-principles, SAPT-based force field.

Relevant Literature

- VanVleet2016: 10.1021/acs.jctc.6b00209
- VanVleet2017: TBA
- McDaniel2013: 10.1021/jp3108182
- Schmidt2015: 10.1021/ar500272n
- Yu2011: 10.1021/jp204563n

Overview

To generate a SAPT-based force field, the following inputs are required: 1. Benchmark dimer energies from SAPT, computed for a variety of dimer configurations 2. Long-range multipole moments, induced dipoles, and dispersion parameters, computed from monomer properties (and BS-ISA in particular) 3. Short-range exponents computed from monomer properties (and BS-ISA in particular) 4. Short-range pre-factors fit to dimer energies

The following scripts are designed to simplify (as much as is possible) the workflow for force field generation.

Method

1. Generate the necessary input files upon which the scripts in step #2 depend. The following files must be manually created/edited, and can all be found in the templates subdirectory (with an example set of input files given for the pyridine dimer):
    1. dimer_info.dat
        - For each monomer, list the monomer's name and the charge on the
        - monomer. The appropriate file format should be clear from the pyridine example.
        - In the manner described in dimer_info.dat, list all midbonds that should be added between monomers. Midbonds are important for running accurate SAPT calcuations; see Yu2011 for details.
    2. generate_grid_settings.inp
        - This is the input file for GenerateGridPoints, which generates the dimer configurations for running SAPT calculations. The input file is commented so as to be self-explanatory; you will need to change (at the very least) the 1st, 3rd, and 4th input sections based on the identities of the two monomers
    3. MONA_MONB.inp (where MONA and MONB are replaced by the monomer names listed in dimer_info.dat)
        - This file contains a title line (line 1), and (for each monomer) the number of atoms followed by a list of coordinates in .xyz format. See pyridine_pyridine.inp for an example.

4. MONA.atomtypes, MONB.atomtypes
    - Each .atomtypes file has the format of a .xyz file, where the element names have been replaced by atomtypes. This file will be used to generate the CamCASP input files needed for ISA calculations, and is also necessary for pre-processing the input files for force field fitting.

2. To generate all files necessary to run force field calculations, run the following pre-processing scripts (from this main directory).

```
./scripts/make_geometries.sh

./scripts/get_global_coordinates.py

./scripts/submit_ip_calcs.py
```

(wait until IP calculation is finished)

```
./scripts/make_sapt_ifiles.py

./scripts/make_isa_files.py

./scripts/make_dispersion_files.py
```

3. Submit all SAPT and ISA calculations to relevant locations. At the time of this writing, SAPT calculations should preferably be run on HCTC (Condor). ISA and dispersion calculations should be run on Phoenix using Camcasp 5.8. Copy all output files back to Pople.

4. Workup the results of the SAPT and ISA calculations by running the following post-processing scripts:

```
./scripts/workup_sapt_energies.py

./scripts/workup_dispersion_files.sh
```

(Depending on the force field, dynamic polarizabilities may need to be added to templates/dispersion_base_constraints.index before running this script. See Jesse McDaniel's thesis and \cite{McDaniel2013} for a full description of the paramterization process for dispersion coefficients.)

```
./scripts/workup_drude_files.sh
```

(Depending on the force field, static polarizabilities may need to be added to templates/drude_base_constraints.index before running this script. See Jesse McDaniel's thesis and \cite{McDaniel2013} for a full description of the paramterization process for drude oscillator charges.)

```
./scripts/workup_isa_charges.py

./scripts/workup_isa_exponents.py
```

After running these scripts, you should have the SAPT energies, long-range coefficients, and short-range exponents required to run the force fitting code (which is needed to generate short-range pre-factors, see \cite{VanVleet2016}). The proper running of this code is described in the POInter documentation, see

https://git.chem.wisc.edu/schmidt/force_fields/wikis/home

Overview of Important Files

- dimer_info.dat <- monomer names and midbond positions
- dispersion_template.clt <- CamCASP input file for getting induction and
- dispersion paramters
- generate_grid_settings.inp <- geometry configuration settings
- isa_template.clt <- CamCASP input file for getting ISA exponents
- pbe0_template.com <- DF-DFT-SAPT template for the PBE0 functional
- pyridine.atomtypes <- change elements to atomtypes; only matters for
- dispersion
- pyridine_pyridine.inp <- monomer geometries

For most systems, only dimer_info.dat, the .inp files, and the .atomtypes file will need to be changed. The examples provided for these files should hopefully make the format self-explanatory.

System Requirements

Python dependencies: * numpy * scipy * chemistry (mvanvleet package; not standard, so this needs to be * downloaded and added to your `$PYTHONPATH`)

Figure A.1: An overview of the semi-automated force field development process. The full workflow and required scripts can be found at `https://github.com/mvanvleet/workflow-for-force-fields`.

BIBLIOGRAPHY

[2] Stone, A. J. *The Theory of Intermolecular Forces*, 2nd ed.; OUP Oxford, 2013.

[3] Furukawa, H.; Cordova, K. E.; O'Keeffe, M.; Yaghi, O. M. *Science (80-.).* **2013**, *341*, 1230444–1230444.

[4] Millward, A. R.; Yaghi, O. M. *J. Am. Chem. Soc.* **2005**, *127*, 17998–17999.

[5] Dietzel, P. D. C. et al. *J. Mater. Chem.* **2009**, *19*, 7362.

[6] Dzubak, A. L.; Lin, L.-C.; Kim, J.; Swisher, J. a.; Poloni, R.; Maximoff, S. N.; Smit, B.; Gagliardi, L. *Nat. Chem.* **2012**, *4*, 810–816.

[7] Czaja, A. U.; Trukhan, N.; Müller, U. *Chem. Soc. Rev.* **2009**, *38*, 1284.

[8] Krishna, R.; van Baten, J. M. *Phys. Chem. Chem. Phys.* **2011**, *13*, 10593–10616.

[9] Getman, R. B.; Bae, Y.-s.; Wilmer, C. E.; Snurr, R. Q.; Carlo, M. *Adsorpt. J. Int. Adsorpt. Soc.* **2012**, 703–723.

[10] Yazaydin, a. O.; Snurr, R. Q.; Park, T.-H.; Koh, K.; Liu, J.; Levan, M. D.; Benin, A. I.; Jakubczak, P.; Lanuza, M.; Galloway, D. B.; Low, J. J.; Willis, R. R. *J. Am. Chem. Soc.* **2009**, *131*, 18198–9.

[11] Valenzano, L.; Civalleri, B.; Chavan, S.; Palomino, G. T.; AreaÌ'n, C. O.; Bordiga, S. *J. Phys. Chem. C* **2010**, *114*, 11185–11191.

[12] McDaniel, J. G.; Schmidt, J. R. *J. Phys. Chem. C* **2012**, *116*, 14031–14039.

[13] McDaniel, J. G.; Yu, K.; Schmidt, J. R. *J. Phys. Chem. C* **2012**, *116*, 1892–1903.

[14] McDaniel, J. G.; Li, S.; Tylianakis, E.; Snurr, R. Q.; Schmidt, J. R. *J. Phys. Chem. C* **2015**, *119*, 3143–3152.

[15] Lao, K. U.; Schaeffer, R.; Jansen, G.; Herbert, J. M. *J. Chem. Theory Comput.* **2015**, 150417132228001.

[16] Pastorczak, E.; Corminboeuf, C. *J. Chem. Phys.* **2017**, *146*, 120901.

[17] Żuchowski, P. *Chem. Phys. Lett.* **2008**, *450*, 203–209.

[18] Horn, P. R.; Head-gordon, M. *Phys. Chem. Chem. Phys.* **2016**, *18*, 23067–23079.

[19] Su, P.; Li, H. *J. Chem. Phys.* **2009**, *131*, 014102.

[20] Chen, Y.; Li, H. *J. Phys. Chem. A* **2010**, *114*, 11719–24.

[21] Su, P.; Jiang, Z.; Chen, Z.; Wu, W. *J. Phys. Chem. A* **2014**, *118*, 2531–42.

[22] Fedorov, D. G.; Kitaura, K. **2006**,

[23] McDaniel, J. G.; Schmidt, J. R. *J. Phys. Chem. A* **2013**, *117*, 2053–2066.

[24] McDaniel, J. G. Development and Application of Physically-Motivated First-Principles Force Fields for Complex Chemical Systems. Ph.D. thesis, UW-Madison, 2014.

[25] Yu, K.; Kiesling, K.; Schmidt, J. R. **2012**,

[26] Verma, P.; Xu, X.; Truhlar, D. G. **2013**,

[27] Valenzano, L.; Civalleri, B.; Sillar, K.; Sauer, J. **2011**, 21777–21784.

[28] Haldoupis, E.; Borycz, J.; Shi, H.; Vogiatzis, K. D.; Bai, P.; Queen, W. L.; Gagliardi, L.; Siepmann, J. I. *J. Phys. Chem. C* **2015**, *74*, 150616135429005.

[29] Yu, K.; McDaniel, J. G.; Schmidt, J. R. *J. Phys. Chem. B* **2011**, *115*, 10054–10063.

[30] Jansen, G.; Scha, R. **2012**,

[31] Guibas, L. Representing rotations with quaternions. 1992; `graphics.stanford.edu/courses/cs164-09-spring/Handouts/handout12.pdf`.

[32] Shoemake, K. *Graph. Gems 3*; 1992; Chapter 6, pp 124–132.

[33] Jeziorski, B.; Moszynski, R.; Szalewicz, K. *Chem. Rev.* **1994**, *94*, 1887–1930.

[34] Szalewicz, K. *Wiley Interdiscip. Rev. Comput. Mol. Sci.* **2012**, *2*, 254–272.

[35] Knizia, G.; Adler, T. B.; Werner, H.-J. *J. Chem. Phys.* **2009**, *130*, 054104.

[36] Misquitta, A. J.; Stone, A. J. CamCASP: a program for studying intermolecular interactions and for the calculation of molecular properties in distributed form, version 5.8. University of Cambridge, 2015.

[37] Stone, A. J. *J. Chem. Theory Comput.* **2005**, *1*, 1128–1132.

[38] Misquitta, A. J.; Stone, A. J.; Fazeli, F. *J. Chem. Theory Comput.* **2014**, *10*, 5405–5418.

[39] Misquitta, A. J.; Stone, A. J. *J. Chem. Phys.* **2006**, *124*, 024111.

[40] Van Vleet, M. J.; Misquitta, A. J.; Stone, A. J.; Schmidt, J. R. *J. Chem. Theory Comput.* **2016**, *12*, 3851–3870.

[41] Cardamone, S.; Hughes, T. J.; Popelier, P. L. a. *Phys. Chem. Chem. Phys.* **2014**, *16*, 10367.

[42] Kramer, C.; Spinn, A.; Liedl, K. R. *J. Chem. Theory Comput.* **2014**, *10*, 4488–4496.

[43] Dixon, R. W.; Kollman, P. a. *J. Comput. Chem.* **1997**, *18*, 1632–1646.

[44] Chaudret, R.; Gresh, N.; Cisneros, G. A.; Scemama, A.; Piquemal, J.-p. *Can. J. Chem.* **2013**, *91*, 804–810.

[45] Unke, O. T.; Devereux, M.; Meuwly, M. *J. Chem. Phys.* **2017**, *147*, 161712.

[46] Ferenczy, G. G.; Winn, P. J.; Reynolds, C. a. *J. Phys. Chem. A* **1997**, *101*, 5446–5455.

[47] Williams, G. J.; Stone, A. J. *J. Chem. Phys.* **2003**, *119*, 4620–4628.

[48] Misquitta, A. J.; Stone, A. J. *Mol. Phys.* **2008**, *106*, 1631–1643.

ACRONYMS

A | C | D | F | I | M | P | S

Symbols

δHF Delta-Hartree Fock. 16, 18

A

AIM atom-in-molecule. 45, 46, 51

C

CUS Coordinatively-Unsaturated. iv, 10, 11, 13–15, 26–28

D

DFT Density Functional Theory. 11, 13–15, 26, 39

DFT-SAPT Density Functional Theory Symmetry-Adapted Perturbation Theory. 11–13, 16, 17, 20, 27, 28, 36, 39, 40, 52

DMA Distributed Multipole Analysis. v, vii, 12, 18, 41, 42, 45–55

E

EDA Energy Decomposition Analysis. 14, 15, 26–28

F

FDDS frequency-dependent density susceptibility. 50

I

isa Iterated Stockholder Atoms. v, vii, 36, 41–43, 45, 47, 50–54, 59, *Glossary:* ISA

M

MOF Metal-Organic Framework. iv, 9–15, 26–28

P

PES potential energy surface. viii, 9, 12, 16, 17, 23, 24, 35–38, 75

POInter **P**arameter **O**ptimizer for **Inter**-molecular Force Fields. 34, 45, 52

S

SAPT Symmetry-Adapted Perturbation Theory. v, viii, 9, 11–16, 18, 26–28, 34–36, 39, 40, *Glossary:* SAPT

GLOSSARY

C | H | I | L | P | S

C

CCSD(T) Coupled Cluster methods including singles, doubles, and perturbative triples excitations. CCSD(T). Given a sufficiently large (aVQZ or better) basis set, can be used as a 'gold-standard' estimate of the exact potential energy surface. v, 9, 13, 28, 36, 40, 41

CCSD(T)-f12 Explicitly-correlated CCSD(T). Given a sufficiently large (aVDZ or aVTZ) basis set, used throughout this work as a 'gold-standard' estimate of the exact potential energy surface. 12–14, 19, 20, 36, 40, 41

H

hetero-monomeric FILL . 35

homo-monomeric FILL . 35

I

induction FILL . 16, 18

ISA Iterated Stockholder Atoms,FILL . v, 41

L

LMO-EDA FILL . iv, viii, 9, 15–20, 23, 25–28

P

POInter FILL . 34

S

SAPT Symmetry-Adapted Perturbation Theory, a perturbative treatment of intermolecular interactions which is pretty cool. v, 9, 34